LEVEL

FINAL REPORT

LOW BAND DUAL MODE TWT

APRIL 1, 1978 TO APRIL 30, 1979

542227

AD A071123

DDC FILE COPY

W-05082

FINAL REPORT

LOW BAND DUAL MODE TWT

APRIL 1, 1978 TO APRIL 30, 1979

30 APRIL 79

DDC

JUN 26 1979

C

HUGHES AIRCRAFT COMPANY
ELECTRON DYNAMICS DIVISION
3100 WEST LOMITA BOULEVARD
TORRANCE, CALIFORNIA 90509

79 06 25 025

REPORT DOCUMENTATION PAGE	READ INSTRUCTIONS BEFORE COMPLETING FORM

1. REPORT NUMBER	2. GOVT ACCESSION NO.	3. RECIPIENT'S CATALOG NUMBER

4. TITLE (and Subtitle)	5. TYPE OF REPORT & PERIOD COVERED
Final Report Low Band Dual Mode TWT April 1, 1978 to April 30, 1979	Final Report covering period April 1, 1978 to April 30, 1979
	6. PERFORMING ORG. REPORT NUMBER W05082

7. AUTHOR(s)	8. CONTRACT OR GRANT NUMBER(s)
MATTHEW PATTERSON WILLARD SUNDQUIST	N00014-72-C-0205

9. PERFORMING ORGANIZATION NAME AND ADDRESS	10. PROGRAM ELEMENT, PROJECT, TASK AREA & WORK UNIT NUMBERS
Hughes Electron Dynamics Division 3100 W. Lomita Boulevard Torrance, CA 90509	N/A

11. CONTROLLING OFFICE NAME AND ADDRESS	12. REPORT DATE April 1, 1978 to April 30, 1979
Office of Naval Research 800 North Quincy Street, Room 722 Arlington, Virginia 22217	13. NUMBER OF PAGES 73

14. MONITORING AGENCY NAME & ADDRESS(if different from Controlling Office)	15. SECURITY CLASS. (of this report)
Naval Research Laboratory 4555 Overlook Ave., S.W. Washington, D.C. 20375	UNCLASSIFIED
	15a. DECLASSIFICATION/DOWNGRADING SCHEDULE

16. DISTRIBUTION STATEMENT (of this Report)

NRL 5733 Report Distribution List dated 4 March 1975

APPROVED FOR PUBLIC RELEASE
DISTRIBUTION UNLIMITED

17. DISTRIBUTION STATEMENT (of the abstract entered in Block 20, if different from Report)

NRL 5733 Report Distribution List dated 4 March 1975

18. SUPPLEMENTARY NOTES

N/A

EDD-W-05082-F

19. KEY WORDS (Continue on reverse side if necessary and identify by block number)

low band dual mode TWT development program

20. ABSTRACT (Continue on reverse side if necessary and identify by block number)

Several low band dual-mode guns were constructed with various grid configurations using standard grid construction techniques. These were tested in a beam analyzer to determine consistency of performance between guns of the same configuration and also to determine beam characteristics with different grid configurations (e.g. triode versus tetrode). In addition, a program was undertaken to produce low band dual-mode gun grid structures (tetrode) using a new manufacturing technique to increase dimensional accuracy. Two of these assemblies have been built.

DD FORM 1 JAN 73 1473   EDITION OF 1 NOV 65 IS OBSOLETE

TABLE OF CONTENTS

ii

LIST OF ILLUSTRATIONS

LIST OF ILLUSTRATIONS (CONTINUED)

LIST OF ILLUSTRATIONS (CONTINUED)

1.0 INTRODUCTION

This report describes work performed by the Electron Dynamics Division of Hughes Aircraft Company, Torrance, California for the Naval Research Laboratory, Arlington, Virginia. The work was performed under contract number N00014-72-C-0205 and covered a period extending from 1 April 1978 to 30 April 1979. The effort was primarily directed toward improvement of dual mode traveling-wave tubes operating at EH Band frequencies.

A significant problem with the dual mode 572H tube has been the inconsistent performance from identically designed tubes. Such a problem could result from inconsistent gun performance. The purpose of phase VIA was two-fold: To evaluate electron gun performance with respect to repeatability and to further improve a newly developed grid fabrication technique. Beam analysis was performed on several 572H guns, manufactured with the current fabrication technique, to investigate the consistency of gun performance and to evaluate the effects of different grid structures on the beam profiles. Section 3 summarizes the performance of each gun and concludes with a comparison of those results. Second, a new grid fabrication technique was developed to improve the accuracy of the grid locations with respect to one another. Section 4 reviews the details of this method and its associated characteristics.

2.0 DUAL-MODE TETRODE GUNS

2.1 TETRODE OPERATION

Figure 1 shows a schematic of the dual-mode tetrode gun used on the
Hughes single bottle dual-mode (SBDM) TWT's. The function of this gun
is to provide beams with not only different current values for each of
the two modes, but also beams with different diameters. The diameter
of the beam is determined by whether the screen grid is biased off or
has a suitable positive drive voltage applied to it. Biased off, this
grid "screens" out the outer portions of the beam leaving the smaller
diameter beam to provide power for the CW mode of operation. The dif-
ferent beam sizes allow for better focussing with a wider spread in
beam currents (typically .3 Amps to 1.2 Amps) which results, so far,
in 7-8 dB output power pulse-up capability.

2.2 STANDARD TETRODE GRID FABRICATION METHOD

Figure 2 shows a cross-section of a standard tetrode grid assembly.
Basically, it is a stacked assembly which is held together by spring
loading. The control grid is formed and machined as a single piece
part and concentricity is held by the I.D. of the focus electrode. The
screen and shadow grids are each formed, brazed to a support, and then
the grid pattern is machined. Concentricity of these grids depends on
brazing alignment and location in the I.D. of an isolating ceramic.
Spacing is provided by spacers and shims. Finally, azimuthal alignment
is provided by a ceramic pin which goes through all of the piece parts
and locates in a hole in the focus electrode. In spite of tolerances
typically on the order of ±.0005 inches (some are tighter) there are
obvious misalignments when considering grid spacings on the order of a
few mils and grid vane widths of about .002 inches. In addition, assem-
bly time may be as much as 16 hours since some of the parts are selected
at assembly.

2

G6372

FOCUS ELECTRODE

SCREEN
GRID

SHADOW
GRID

CATHODE

ANODE

CONTROL
GRID

CW BEAM   PULSE BEAM
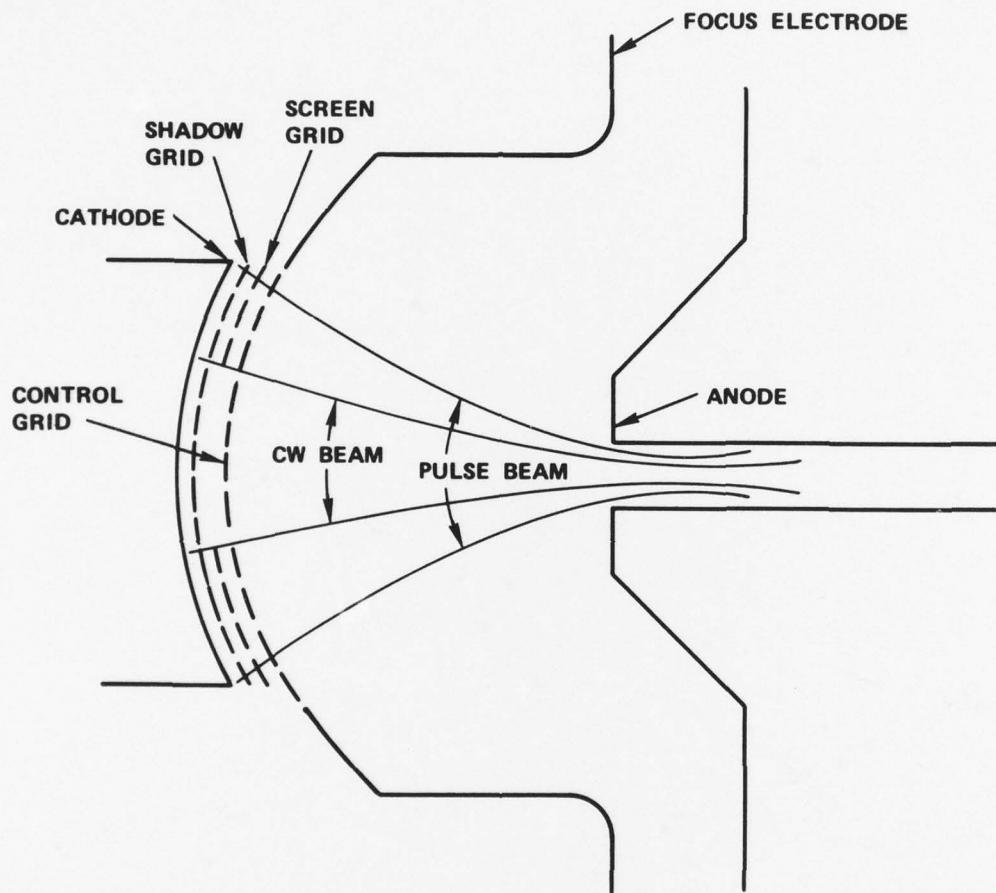
FIGURE 1   DUAL-MODE TETRODE GUN.

3

G6373
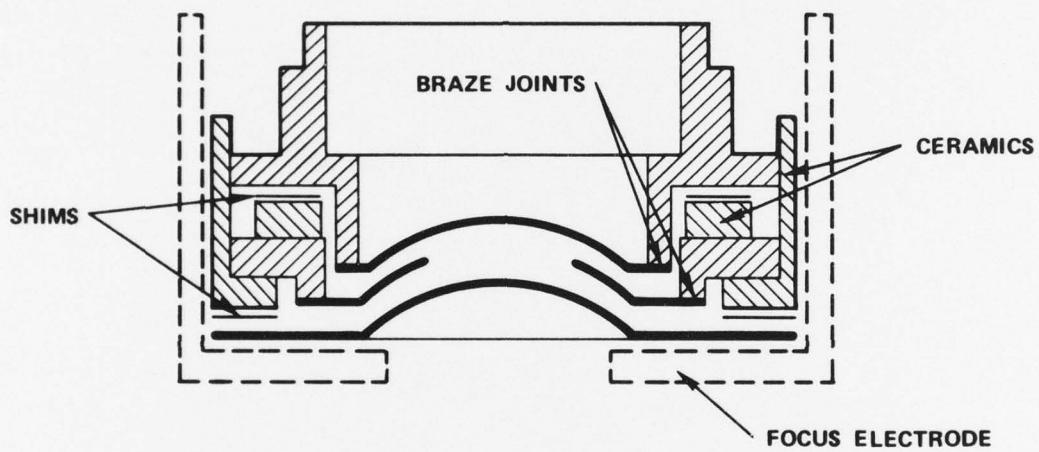
FIGURE 2   STANDARD TETRODE GRID ASSEMBLY CONSTRUCTION.

2.3 TETRODE PERFORMANCE WITH STANDARD GRID ASSEMBLY

One of the problems encountered in the development of the SBDM is performance inconsistencies from tube to tube which do not appear to be the result of circuit design changes. The effects of the design changes have been masked somewhat by inconsistent gun performance. Table 1 shows data collected on the I/J band SBDM which has the same grid construction as in the E/H Band SBDM. Of major interest is the wide range of required grid drive voltages for constant beam currents and the wide range of grid interception currents (i_{c1} & i_{c2}). This data indicates inaccuracies in grid spacings, grid concentricities, and azimuthal grid alignment. These inaccuracies occur in spite of using piece parts with very tight tolerances and a large amount of assembly labor. It was the assembly problems and inconsistencies which lead to the sandwich grid concept and the beam analysis work done on this project.

TABLE 1

I/J BAND SINGLE BOTTLE DUAL-MODE GUN CHARACTERISTICS

S/N	CW Mode (I_k = .30 Amps)		Pulse Mode				
	e_{c2} (V)	i_{c2} (mA)	e_{c1} (V)	e_{c2} (V)	I_k (mA)	i_{c1} (mA)	i_{c2} (mA)
59	295	ϕ	150	295	700	1	7
60	275	ϕ	170	340	1100	22	6
61	360	ϕ	250	465	1000	0	2
62	273	ϕ	250	307	900	6	28
64	225	ϕ	265	320	1100	14	9
66	287	ϕ	133	350	1050	1	13
67	264	ϕ	191	347	1200	7	28

3.0 BEAM ANALYSIS OF GUNS BUILT WITH THE
STANDARD FABRICATION METHOD

Section 3 describes in detail the beam analysis of 2 tetrode guns, a
"vaneless" tetrode, and a triode gun. A diagram of each type of gun is
included showing the relative position of the electrodes. A brief
description of the beam analyzer and its associated apparatus is given.
Beam analysis techniques are described and the results displayed graphi-
cally. Finally, a summary of results is tabulated and a comparison of
gun performances is presented.

3.1 DESCRIPTION OF THE BAKEABLE DEMOUNTABLE ANALYZER

All gun testing was performed on the bakeable demountable analyzer manu-
factured by ETM Electromatic. The analyzer consists of a gun welded to
a bellows assembly containing a tungsten pinhole probe and two collec-
tors (see Figure 3). The interior of the bellows is held under vacuum,
and the entire assembly can be baked-out at $350^{o}C$. The probe is a
tungsten disc with a $0.0035 \pm 0.0005''$ hole in its center. The collec-
tors and probe can be moved as a unit in 3 mutually perpendicular
directions, two across the beam (X and Y sweeps), and one down the beam
axis (Z sweep). When the pinhole is situated in the path of the elec-
tron beam, most of the beam's energy is dissipated in the tungsten disc
which is water cooled via a copper heat sink. A small portion of the
current goes through the pinhole and is captured by the collectors.

The combined current signal from both collectors is delivered to the
amplifier shown in Figure 4. For pulsed operation a "sample and hold"
is used to interface with a chart recorder. The "sample and hold"
transforms the pulsed signal delivered from the amplifier into a DC
voltage porportional to the peak voltage output of the amplifier. The
output of the "sample and hold" drives the vertical motion of the chart
recorder. Consequently, the voltage input to the y-axis of the chart

6

G6374
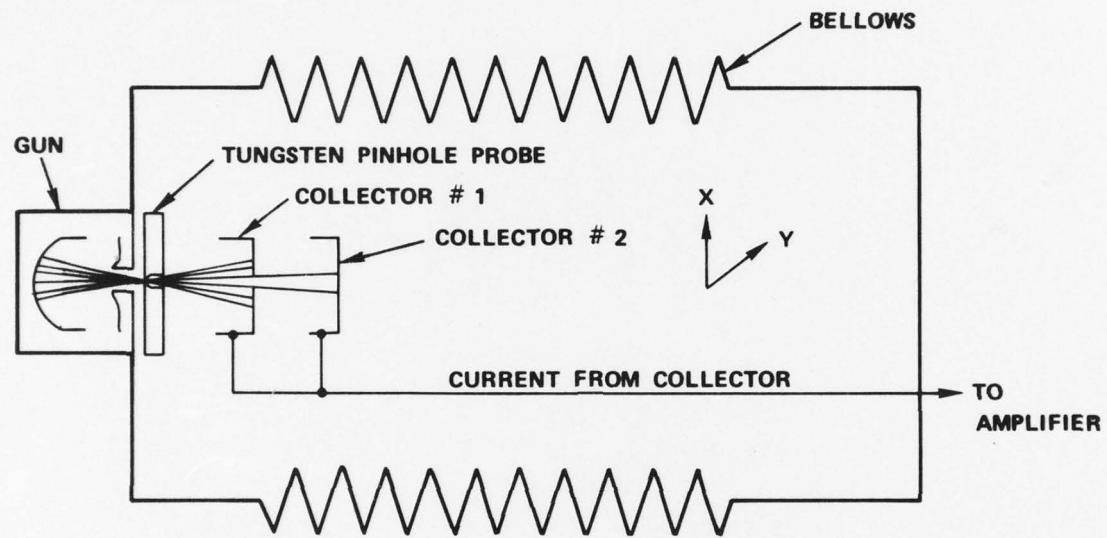
FIGURE 3   BAKEABLE DEMOUNTABLE ANALYZER BELLOWS ASSEMBLY.

G6375
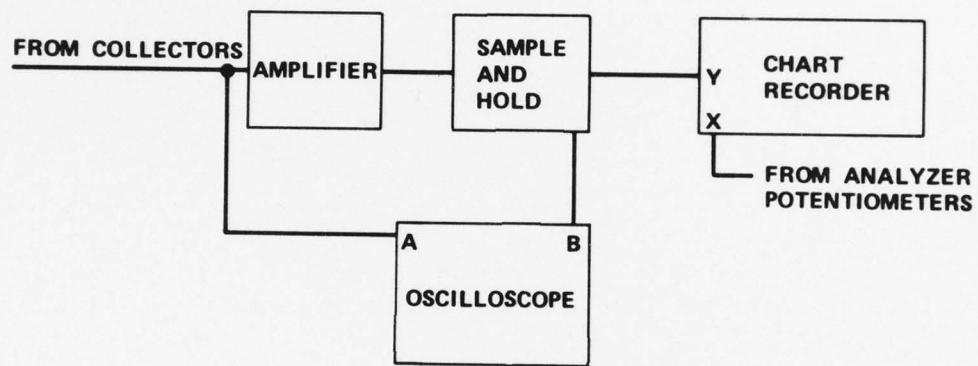
FIGURE 4   TEST APPARATUS.

recorder is proportional to the relative current density in the beam at the pinhole's position.

Beam profiles were taken by sweeping the pinhole across the beam with either the x or y sweep (but not both simultaneously). The above sweep mechanisms are driven automatically, and each is coupled to a potentiometer which drives the horizontal motion of the chart recorder. A typical beam profile is shown in Figure 5. The relative position of the pinhole in the beam is shown on the x-axis calibrated to 0.010"/in. of plot paper. The relative current density is plotted on the y-axis.

3.2 MEASUREMENT OF BEAM DIAMETERS AND BEAM MINIMUM POSITIONS

Before beam diameters were measured, the analyzer was adjusted so that the y-sweep drove the pinhole through beam center. First, a beam profile was taken using the x-sweep with the probe located at an arbitrary axial position. The diameter of this profile was found by drawing a horizontal line at 5% of the peak current density of the beam (see Figure 5). Vertical lines were drawn to the x-axis from the 2 points at which the horizontal intersects the profile. The distance between those vertical lines, according to the x-axis calibration of the chart recorder, is the profile diameter. The center of the profile is defined as the mid-point between the vertical lines. The pinhole was then moved with the x-sweep to the center of the profile. Leaving the x-sweep fixed, a profile was then taken with the y-sweep. The diameter of this profile is the beam diameter at that axial position, since the pinhole swept through beam center.

Most beam diameters were measured using the y-sweep of the analyzer. The x-sweep was adjusted initially, as described above, and left unchanged for all measurements with the y-sweep. However, for each gun a beam diameter was measured with the x-sweep to verify that the beam was cylindrical.

9

G6376
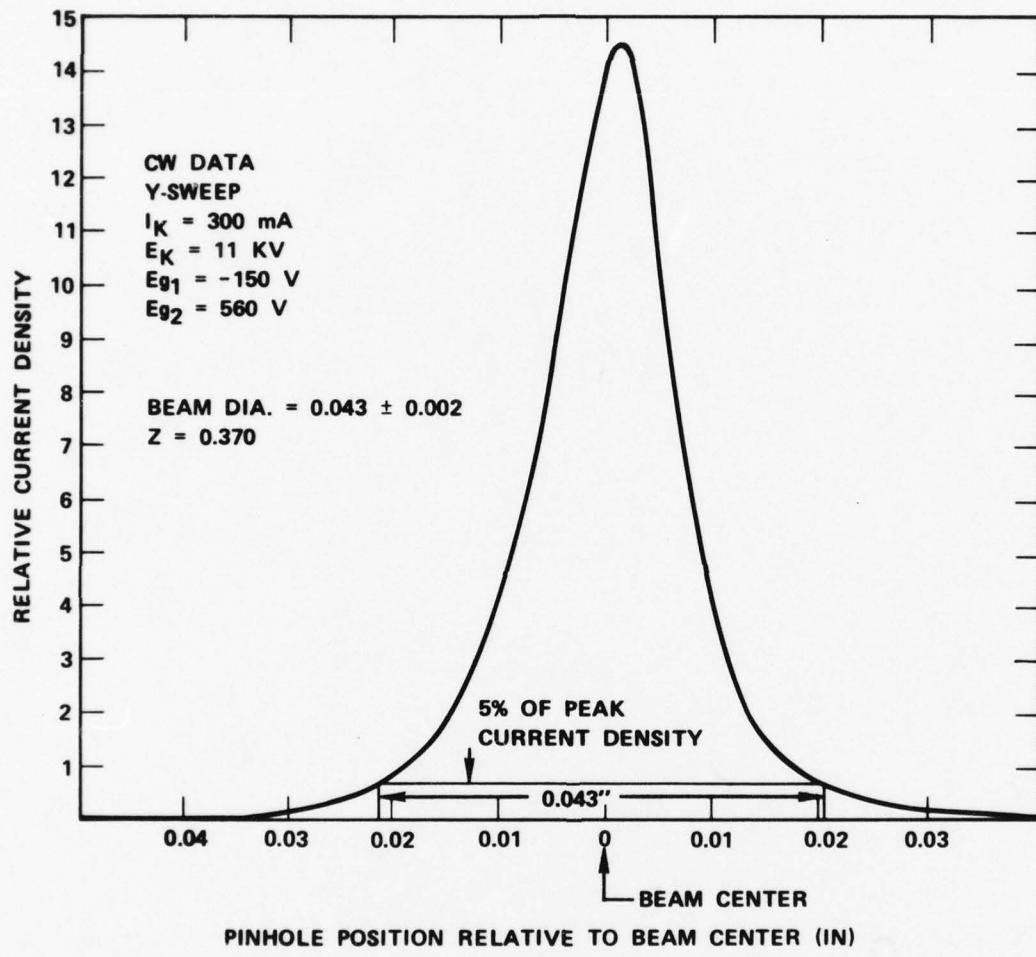
FIGURE 5   CURRENT DENSITY PROFILE FROM TETRODE #2.

10

The profile of Figure 5 was taken with the y-sweep of the analyzer and with the pinhole located 0.370" from the cathode center ($z = 0.370$). The beam minimum position or beam "waist" is that axial position at which the beam diameter is smallest, and the beam minimum diameter is the diameter at the waist. The position of the waist and its diameter were found by taking several profiles, like that in Figure 5, at positions 0.040" apart along the z-axis. In most cases the diameter converged to some minimum value with increasing z, and then diverged as shown in Figure 6.

3.3 ANALYSIS OF TETRODE #1

It should be noted that the beam analyzer pinhole cannot withstand the 3 kW of beam power in the CW mode. Consequently, all data was taken by pulsing the grids with a 0.05% duty cycle. Even with this restriction pinholes made of copper and moly were destroyed by the incident electron beam. Cathode destruction was caused by vaporization of the pinhole material which ultimately poisoned the cathode. Consequently, attempts at analyzing tetrode #1 were unsuccessful.

3.4 ANALYSIS OF TETRODE #2

Analysis of tetrode #2 was successful after the following changes were made. The copper pinhole was replaced by one made of tungsten, and the pulse width was reduced from 5 μsec to 2 μsec with the duty cycle maintained at 0.05%. Reduction of the pulse width cut down on the energy dissipation in the pinhole, per pulse, by 60%. In the CW mode beam minimum diameters were measured at $E_K = 9$, 10 and 11 kV with $I_K = 300$ mA in all cases. The results in Figure 7 show the diameters decreasing linearly with increasing E_K. Such behavior is expected since thermal effects in the beam become less pronounced as the beam energy increases.

11
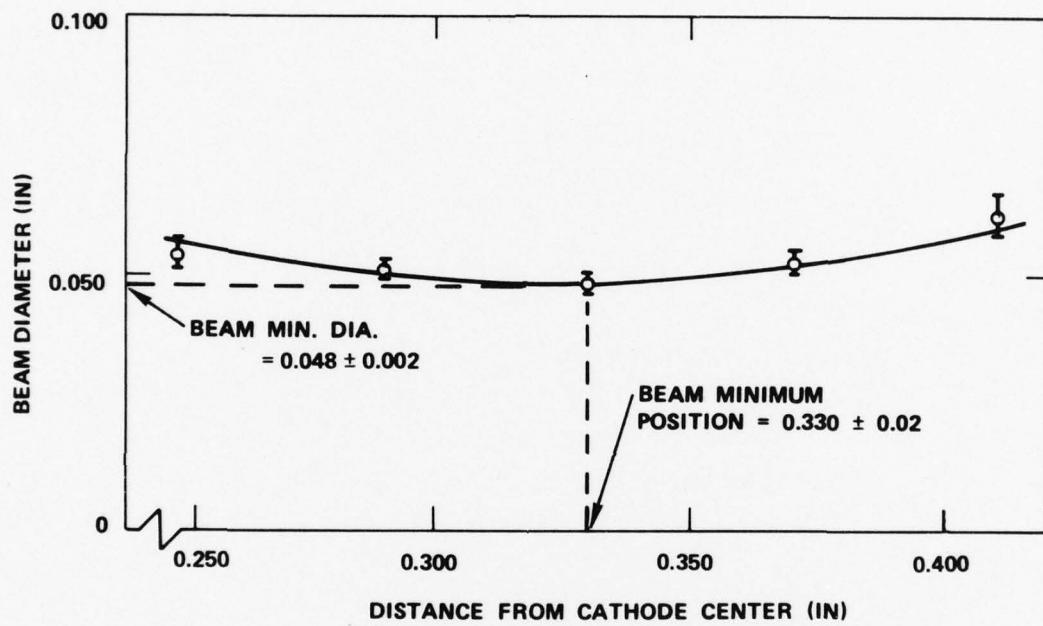
FIGURE 6   DETERMINATION OF A BEAM MINIMUM DIAMETER AND
A BEAM MINIMUM POSITION

G6378
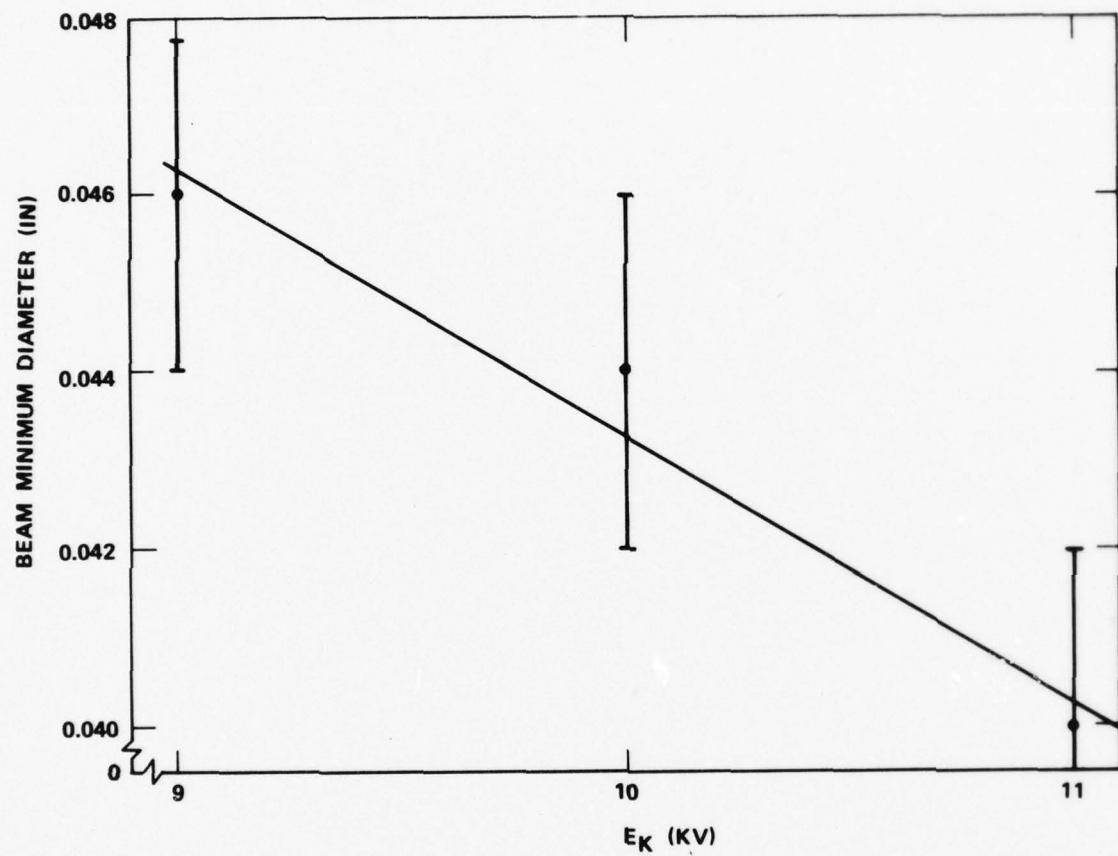
FIGURE 7   CW MODE BEAM MINIMUM DIAMETERS VS. E_k FROM TETRODE #2

13

Figure 8 shows the corresponding CW beam minimum positions plotted as a function of E_K. At both E_K = 9 and 11 kV the positions were 0.320" from the cathode center. However, E_K = 10 kV the position was 0.290" with an uncertainty of ±0.040". The relatively slow variation of beam diameter with axial position caused this large uncertainty.

Figures 9 and 10 show obvious variations in current density for different axial positions. The profile in Figure 9 was taken near the waist, and that in Figure 10 was taken 0.080" closer to the cathode. Typically, all guns, gridded or otherwise, exhibit "hollow" beams between the cathode and waist, due to the perturbation in equipotentials resulting from the hole in the anode. The loading at the cathode center is smaller than near its edges. However, the asymmetry of the profile in Figure 10 is evidence of a crooked grid.

Pulse mode beam minimum diameters were measured at E_K = 9, 10 and 11 kV and I_K = 1.2A with two grid voltage conditions: E_{g1}/E_{g2} = 0.50 and 0.75. Beam minimum diameters as a function of E_K are plotted in Figure 11. In the case where Eg_1/Eg_2 = 0.75 the diameters decreased steadily with increasing E_K. However, an anomalously large diameter was found at E_K = 10 kV when Eg_1/Eg_2 = 0.50. Such a deviation could have resulted from turbulence in the beam caused by the screen and control grids. For each E_K a unique combination of grid voltages Eg_1 and Eg_2 exists such that the grids are on equipotentials. Under these conditions the grids are essentially "invisible" to the beam and cause minimal turbulence. Grid voltages other than the invisible values perturb the equipotentials creating non-laminar trajectories.

Examination of the pulse mode profiles of Figures 12 and 13 reveals a large current density in the outer edge of the beam. The shaded areas, called the beam "tails" contain roughly 14% of the total beam current in Figure 13, and 8% in Figure 12. Furthermore, note that the percentage of current in the tails increases as Eg_1/Eg_2 increases. This behavior is expected since more current is drawn from the cathode edges as this ratio increases.

14

G6379
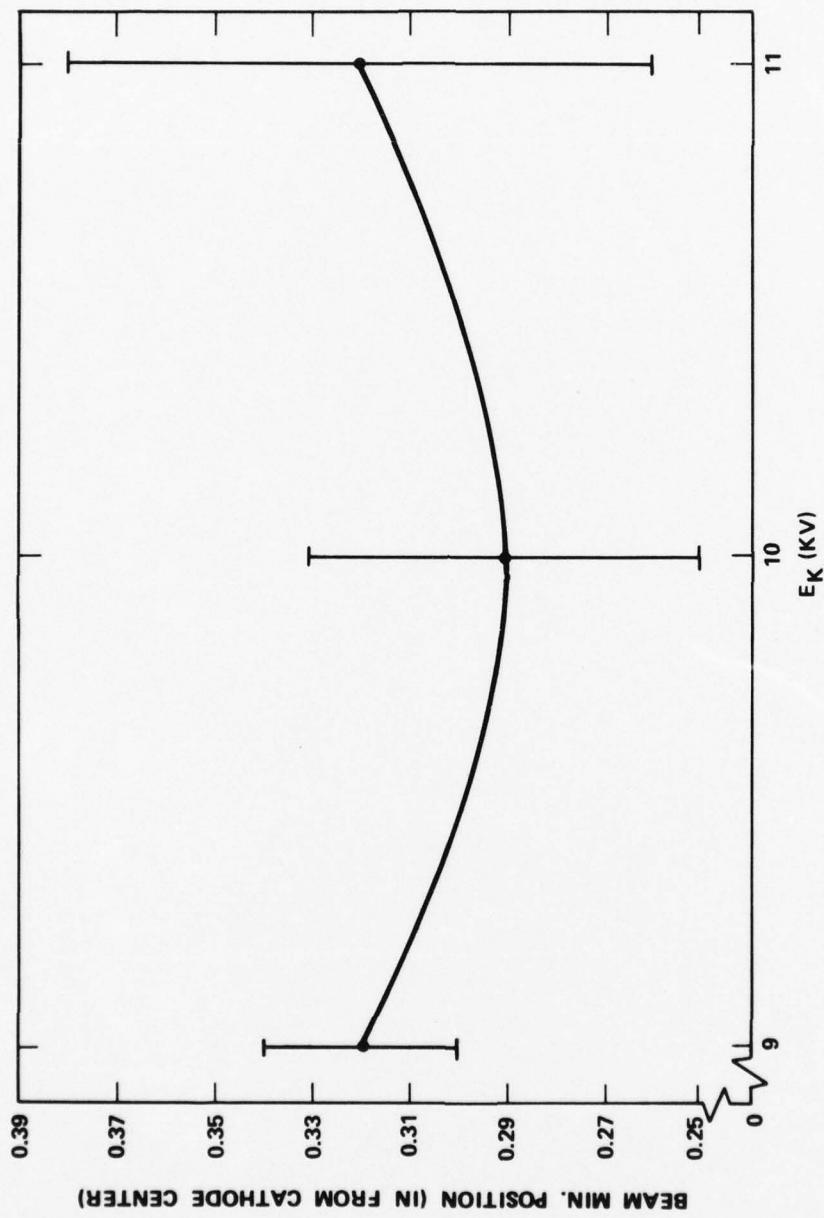
FIGURE 8 CW MODE BEAM MINIMUM POSITION VS. E_k FROM TETRODE #2

15
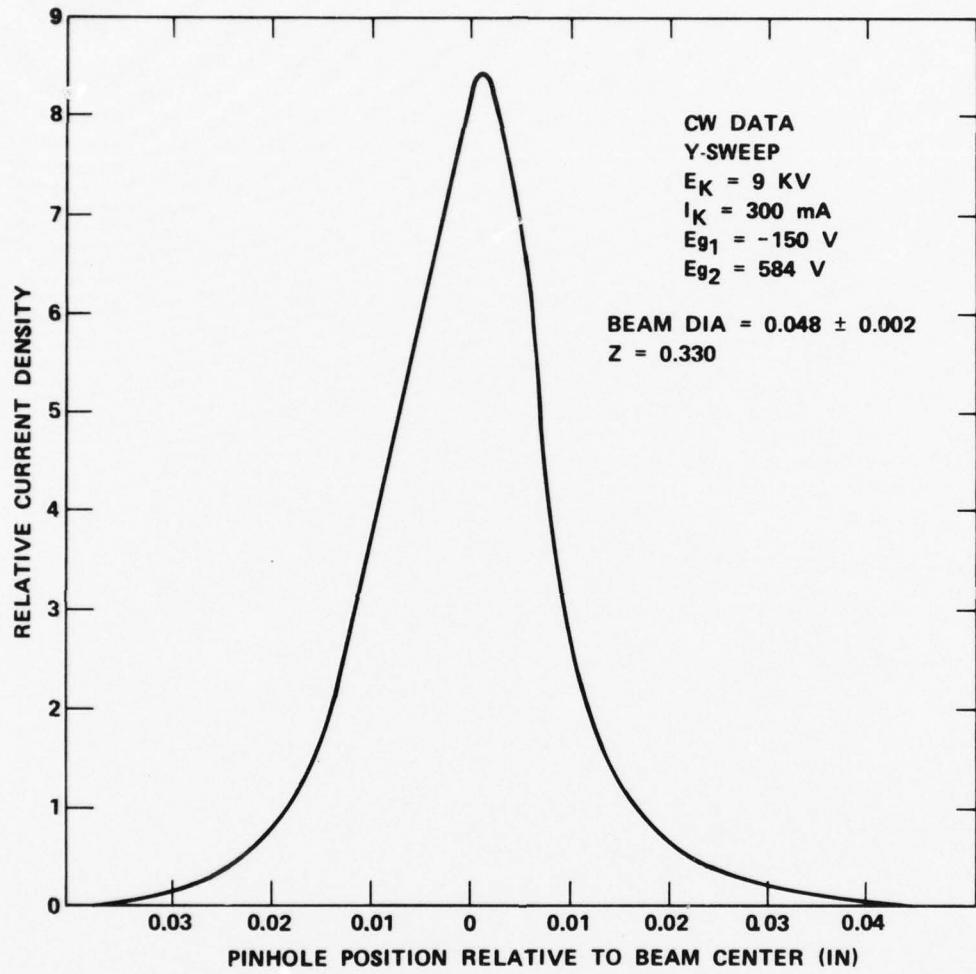
FIGURE 9   PROFILE FROM TETRODE #2 TAKEN AT BEAM WAIST
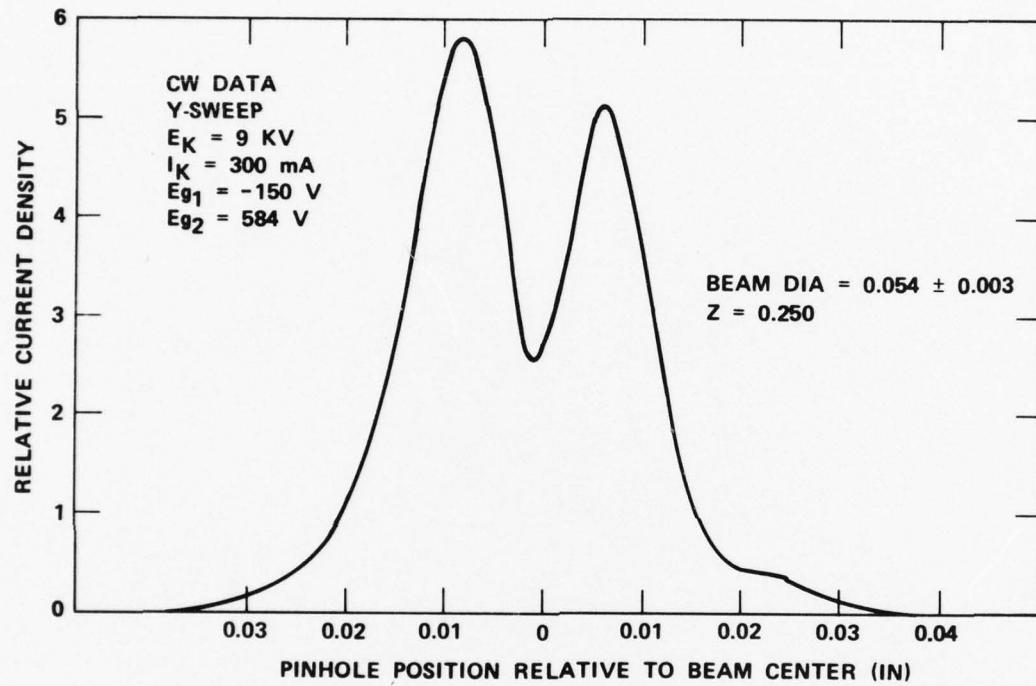
FIGURE 10   PROFILE FROM TETRODE #2 ILLUSTRATING
ASYMMETRIC HOLLOW BEAM
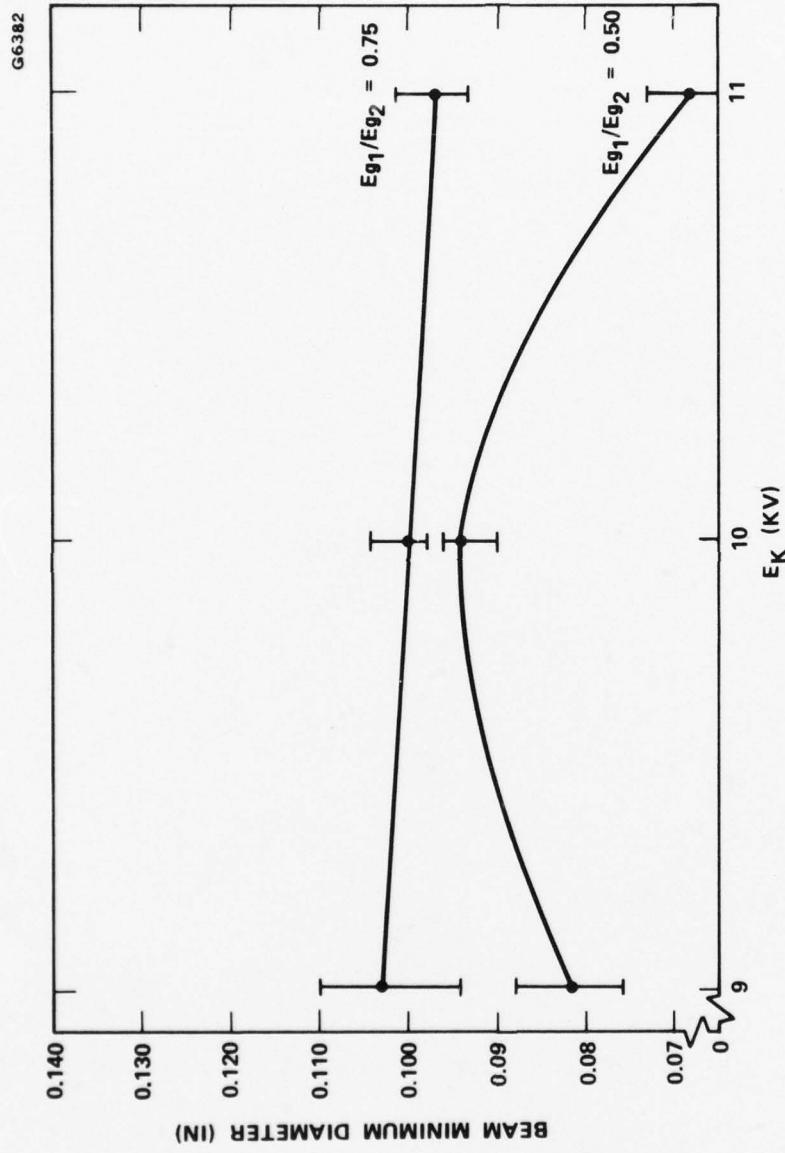
FIGURE 11   PULSE MODE BEAM MINIMUM DIAMETER VS. E_k FROM TETRODE #2

18
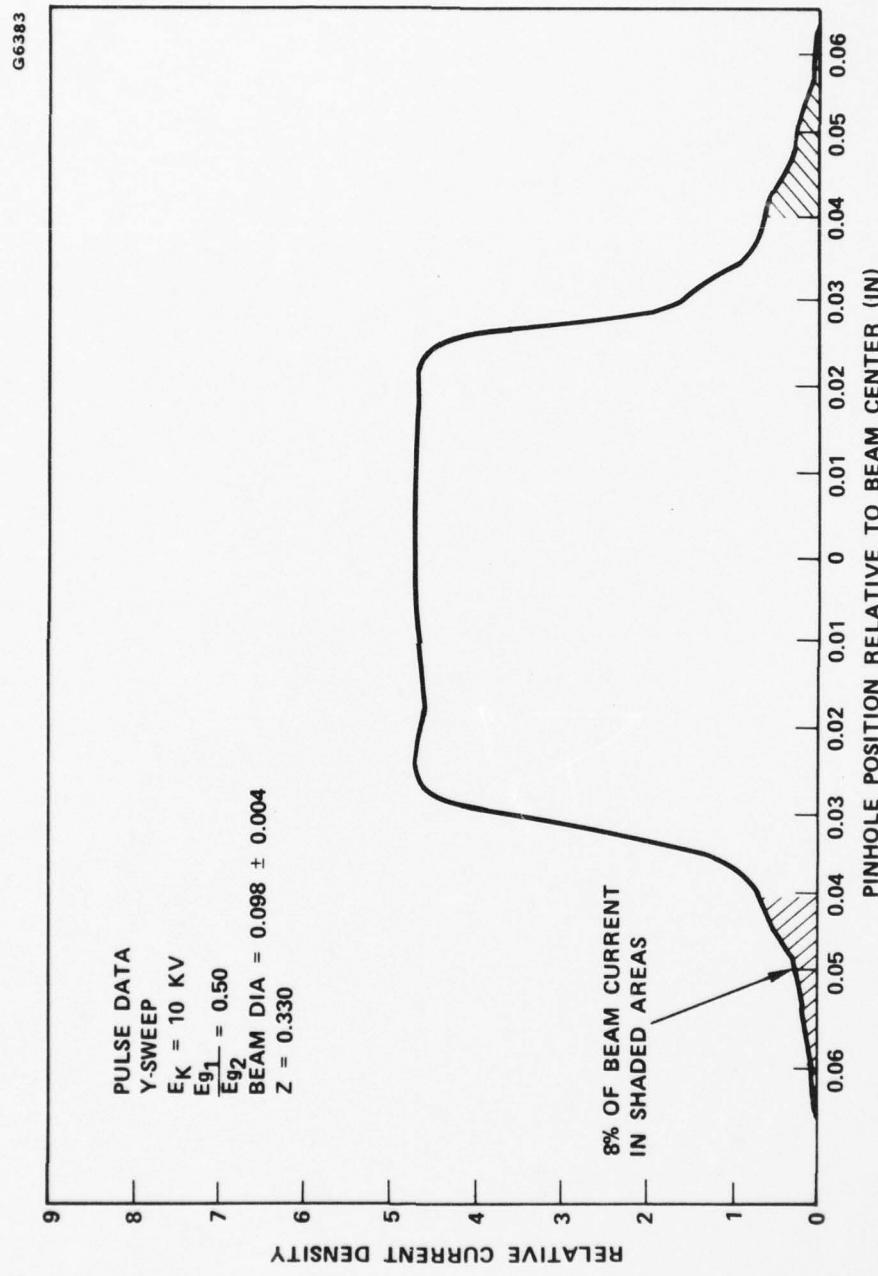
FIGURE 12   PROFILE FROM TETRODE #2 ILLUSTRATING TAILS WITH E_{g1}/E_{g2} = .50

19
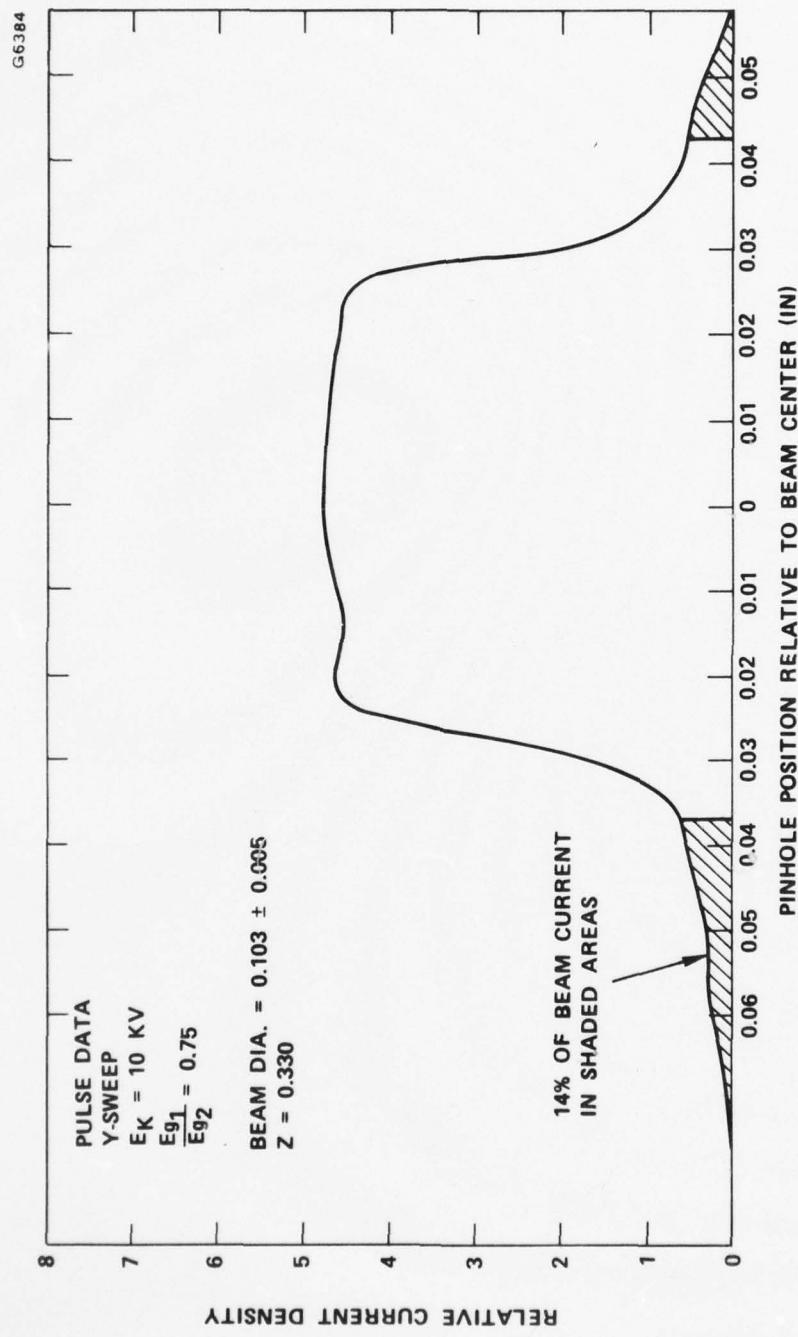
FIGURE 13 PROFILE FROM TETRODE #2 ILLUSTRATING TAILS WITH E_{g1}/E_{g2} = .75

Pulse mode beam minimum positions are plotted as a function of E_K in Figure 14. An anomalous position was found at E_K = 10 kV and Eg_1/Eg_2 = 0.50. Non-laminar beams exhibit anomalies in both diameter and waist location, since they contain trajectories which are crossing each other in an undetermined fashion.

3.5 ANALYSIS OF TETRODE #3

To evaluate the effects of the screen grid on beam diameters and profiles, a "vaneless" tetrode gun was analyzed. The electrodes of tetrode gun #3 were constructed as shown in Figure 15. A vaneless, annular screen grid was used instead of the standard screen grid. Removal of the grid vanes allowed electron emission from nearly the entire cathode surface in both CW and pulse modes.

Data was taken in a similar fashion to that for tetrode #2. For the CW mode, beam minimum diameters and positions were measured at E_K = 9, 10 and 11 kV, I_K = 300 mA and Eg_1 = -150V. Figure 16 shows the beam minimum diameter increasing steadily with increasing E_K. The beam profile at the waist was peaked for all E_K, but it was asymmetric at other axial positions. A typical example of this asymmetry is shown in Figure 17. A crooked control grid could account for this asymmetry. The beam minimum position for the CW mode was constant at 0.335" from the cathode center for all values of E_K (see Figure 18).

Pulse mode data was again taken at E_K = 9, 10, and 11 kV, I_K = 1.2A, and with Eg_1/Eg_2 = 0.50 and 0.75. Figure 19 shows the behavior of the beam minimum diameter as a function of E_K. In both cases (Eg_1/Eg_2 = 0.50 and 0.75) the diameters decrease with increasing E_K. The beam minimum position in all cases was 0.335", identical to that in the CW mode (see Figure 20).

G6385
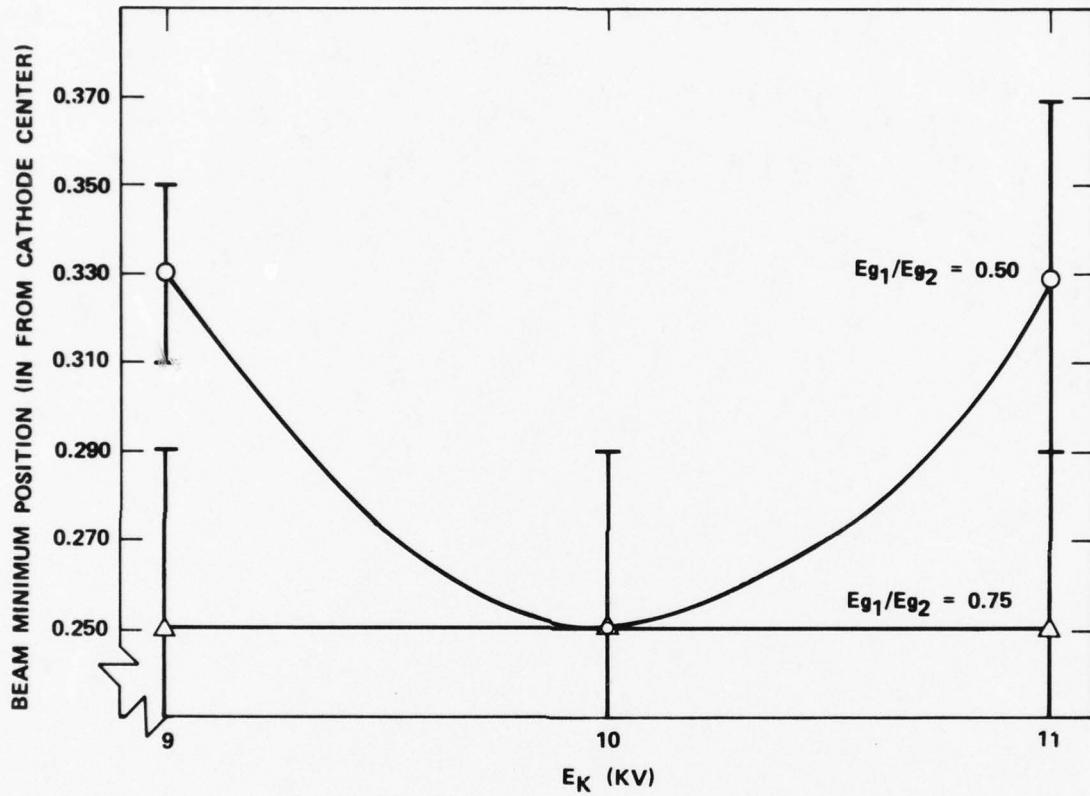
FIGURE 14   PULSE MODE BEAM MINIMUM POSITIONS VS. E_k FROM TETRODE #2

22

G6386
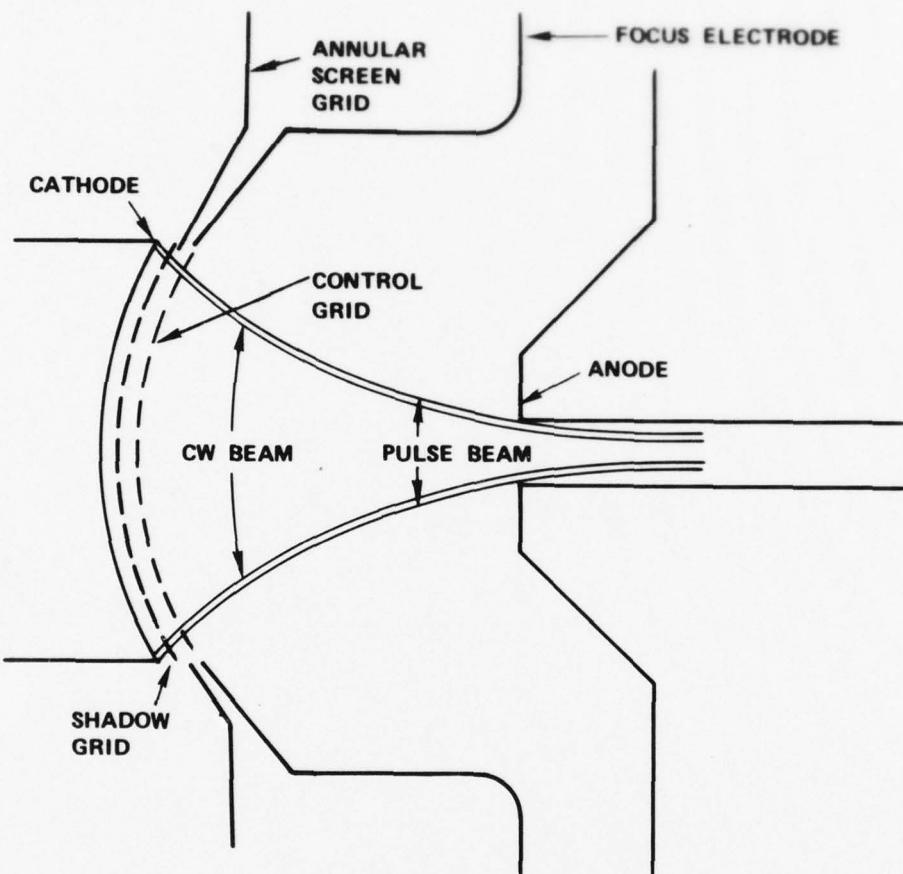
FIGURE 15   ELECTRODE CONFIGURATION OF A VANELESS TETRODE GUN

23
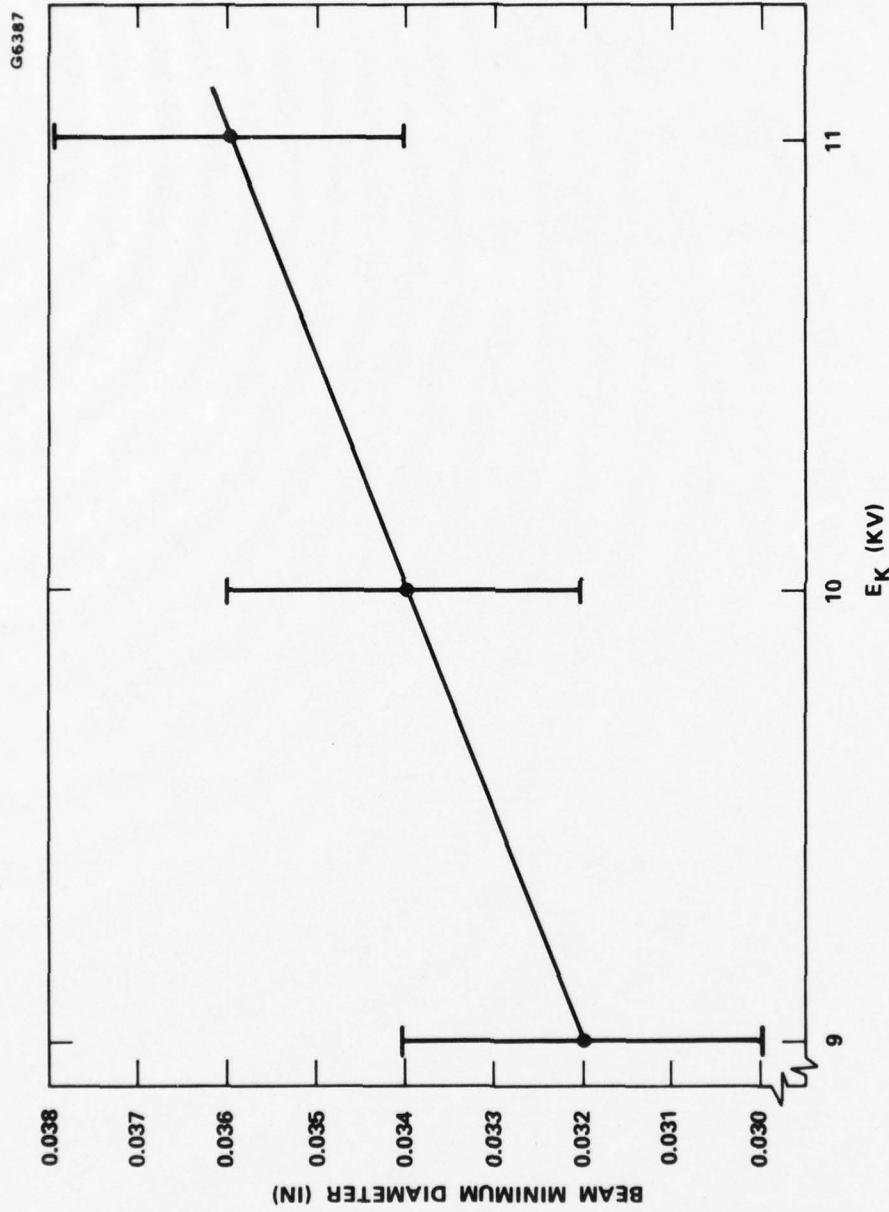
FIGURE 16 CW MODE BEAM MINIMUM DIAMETERS VS. E_k FROM TETRODE #3

24

G6388
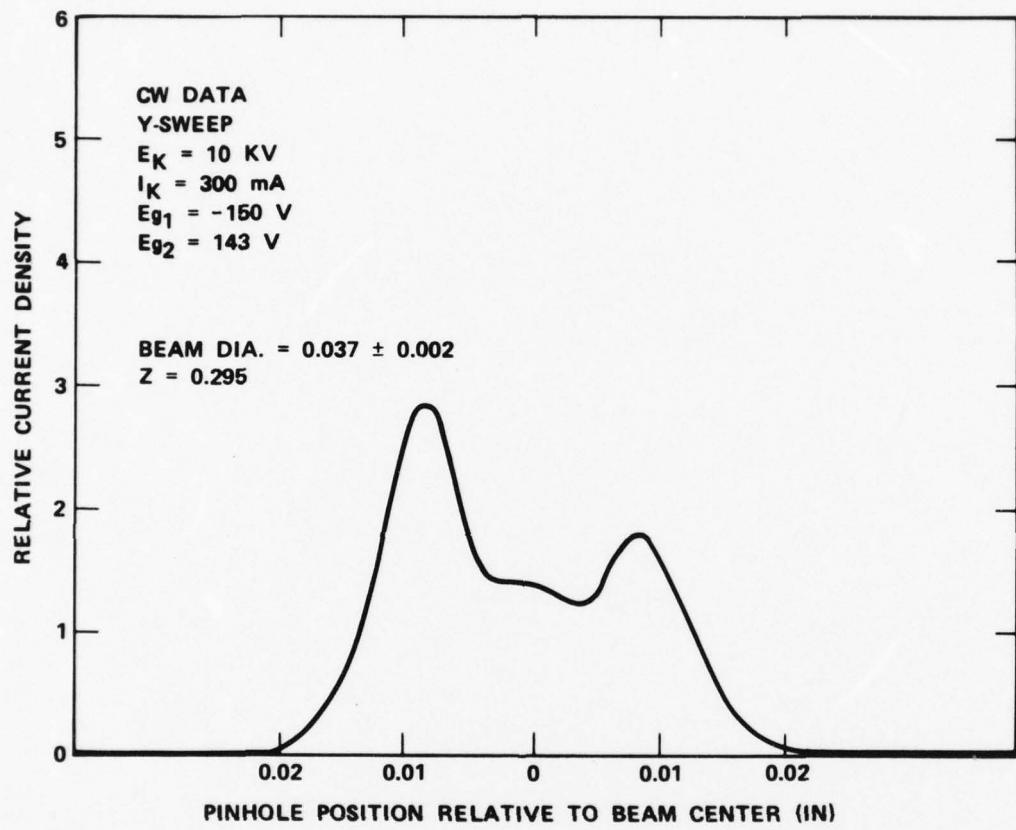
FIGURE 17   PROFILE FROM TETRODE #3 ILLUSTRATING
ASYMMETRIC HOLLOW BEAM
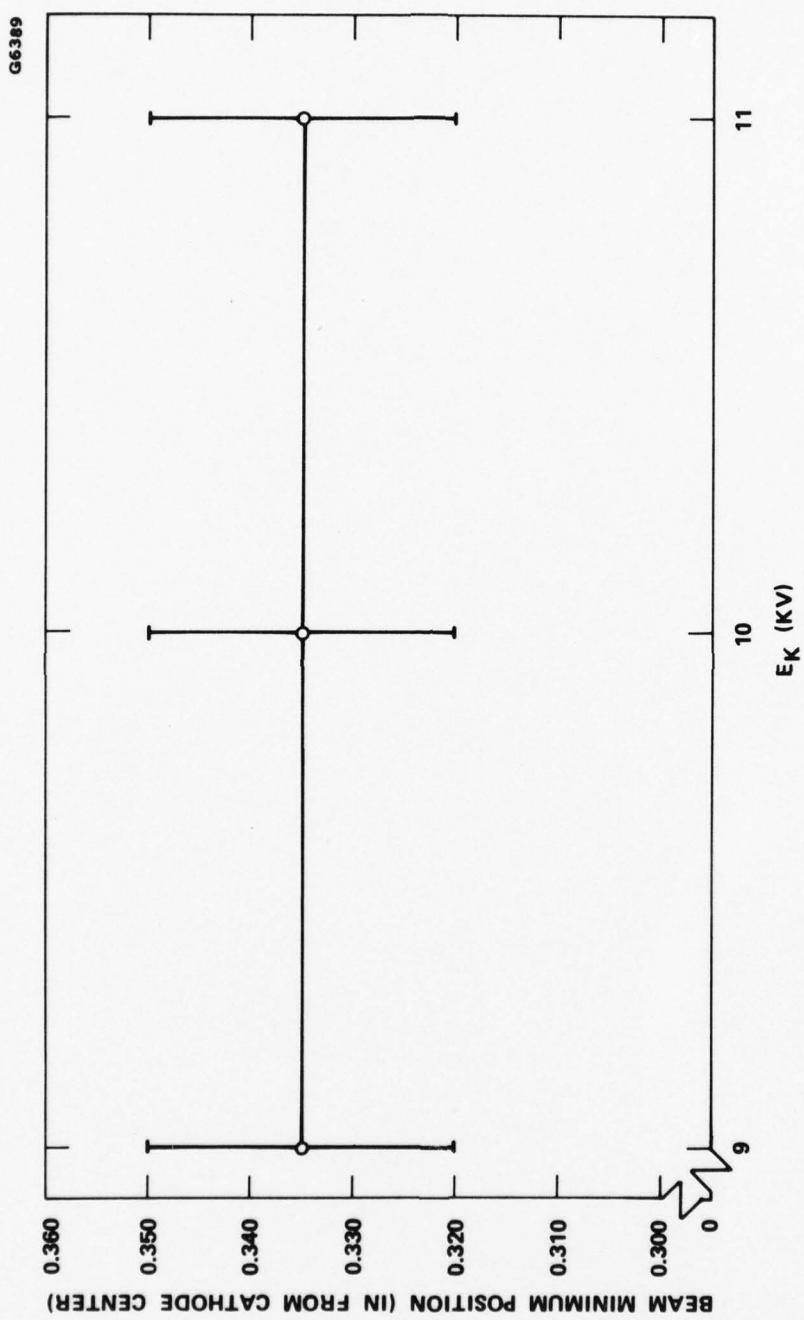
FIGURE 18   CW MODE BEAM MINIMUM POSITION VS. E_k FROM TETRODE #3

26
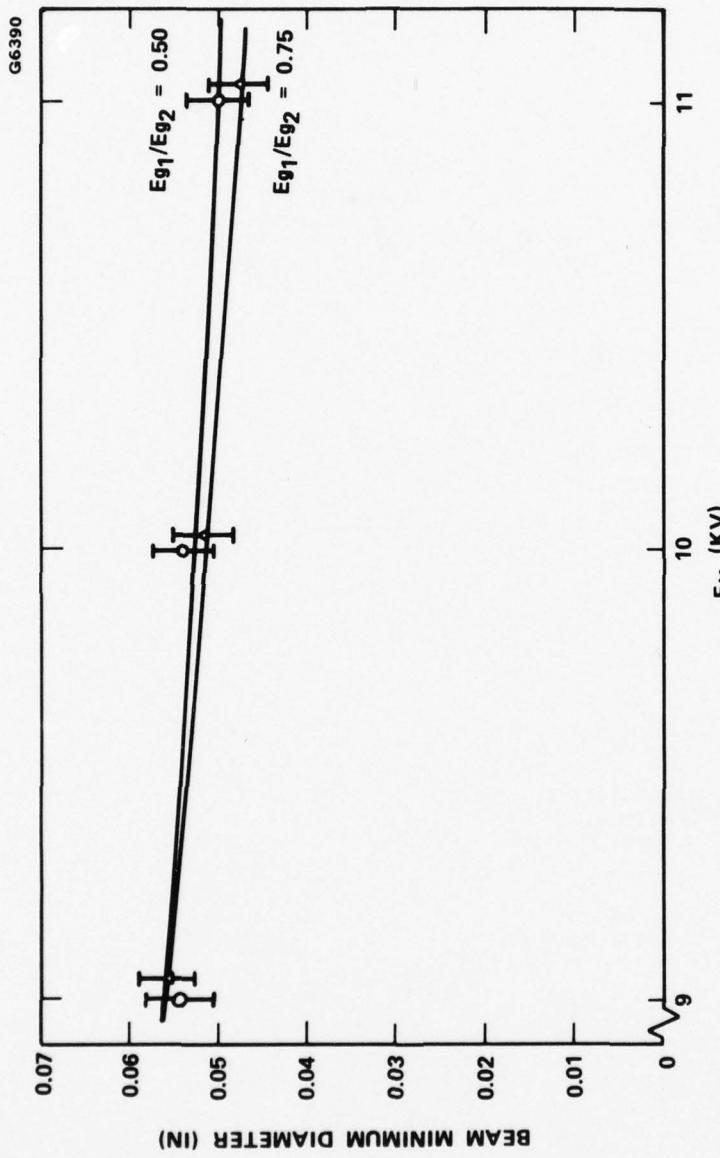
FIGURE 19   PULSE MODE BEAM MINIMUM DIAMETERS VS. E_k FROM TETRODE #3

27

G6391
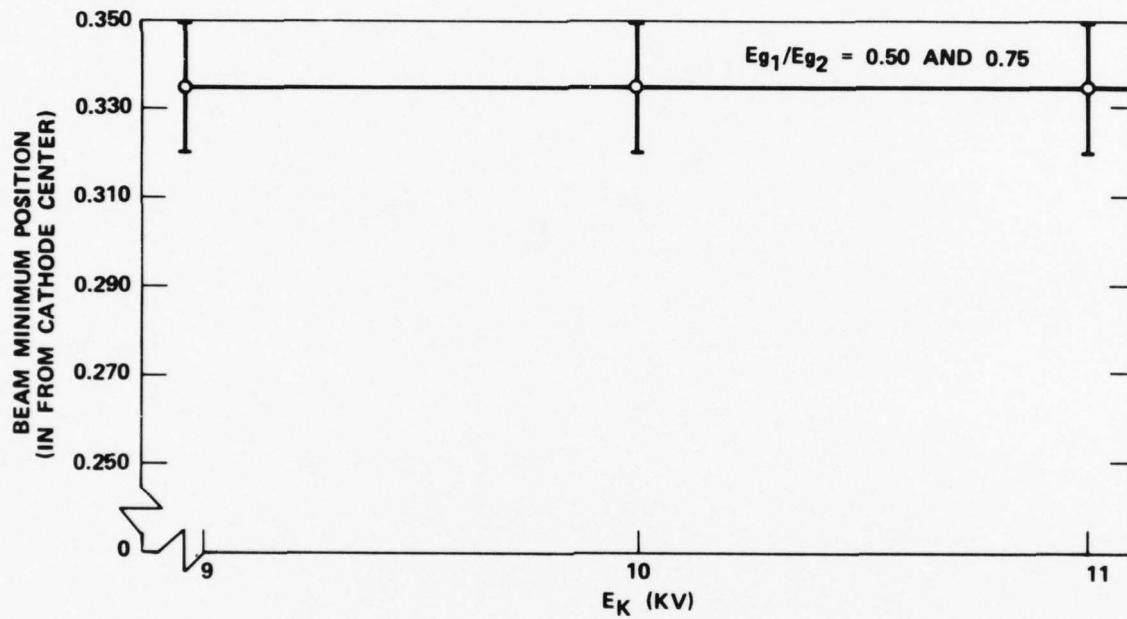
FIGURE 20   PULSE MODE BEAM MINIMUM POSITIONS VS. E_k FROM TETRODE #3

28

A typical profile in the pulse mode is shown in Figure 21. The percentage of current in the tails (shaded areas) is 5%. Since the screen grid was modified as described previously, little or no change was observed when Eg_1/Eg_2 was changed from 0.75 to 0.50. Furthermore, comparing this profile to that in Figure 13 indicates that eliminating the screen grid changed the shape of the profile and reduced the percentage of current in the tails.

3.6 SYSTEM AND DATA ANALYSIS IMPROVEMENTS

In all three of the guns previously discussed, there was evidence of cathode poisoning. Grid voltages were 50 to 100% larger than their design values. The tungsten pinhole experienced excessive heating during operation of the analyzer, indicated by the discoloration of the probe surface. Even though the pinhole diameter remained relatively constant, material was probably ionized from the probe surface. If ions entered the region between the cathode and anode, they experienced an acceleration toward the cathode, bombarded the cathode and ultimately poisoned it.

Before tetrode #4 was tested two improvements were made to remedy this problem known as ion focussing. First, a 2 ℓ/sec ion pump was added to the system. Previously, the system contained a 0.2 ℓ/sec ion pump at the opposite end of the bellows assembly from the gun. With a dispenser cathode, pressures should be maintained below 10^{-6} Torr to avoid poisoning. Such pressures are outside the range of 0.2 ℓ/sec pump. An order of magnitude pressure gradient exists between the two ends of the bellows assembly when under vacuum. Thus, the new pump was located directly behind the gun, welded to its seal cap, so that the pressure at the cathode could be monitored more accurately.

The second improvement was in the method of obtaining and analyzing the data. Beam profiles were taken with $E_K \leq 4$ kV, and the results were
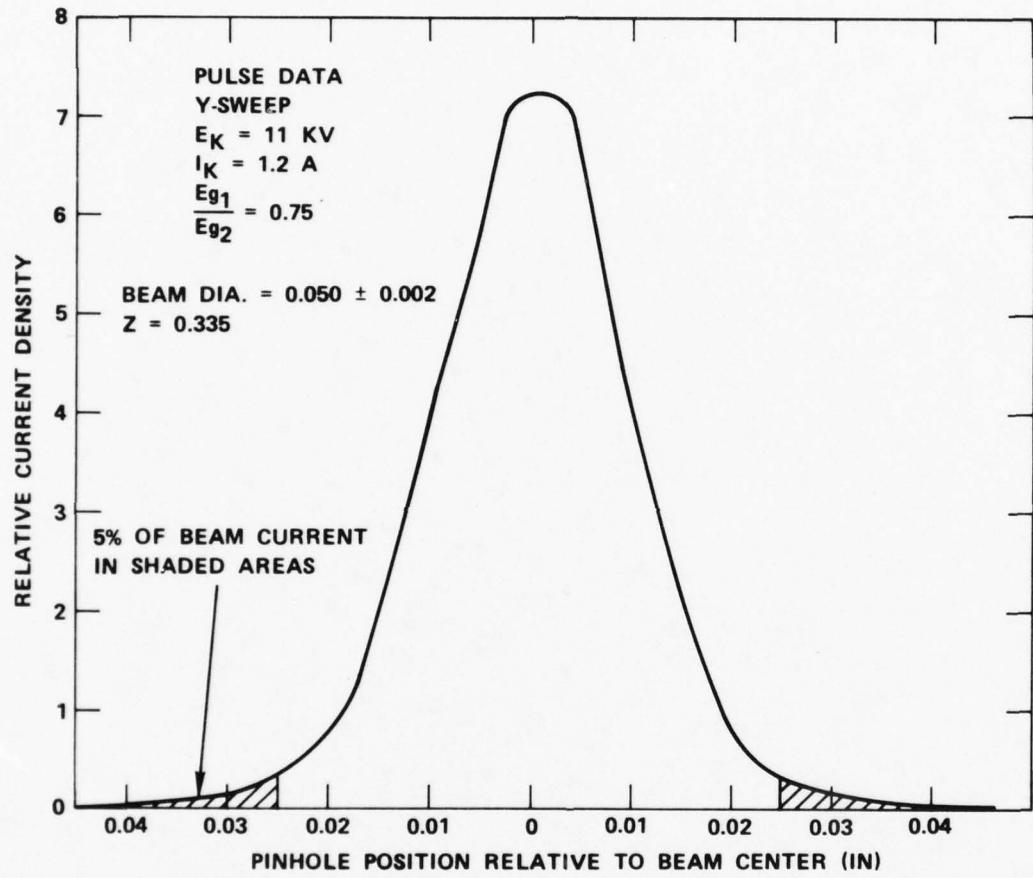
FIGURE 21 PROFILE FROM TETRODE #3 ILLUSTRATING
TAILS WITH E_{g1}/E_{g2} = .75

extrapolated to the higher voltages of E_K = 9, 10 and 11 kV. At the lower voltages ion focussing was not present and cathode poisoning was avoided.

Two different methods were used to find the extrapolated beam diameters. Beam minimum diameters and positions were measured in the same fashion as before for several values of $E_K \leq 4$ kV. For each value of E_K the beam current was adjusted by applying the appropriate grid voltages to maintain a constant perveance beam. Under these conditions it is known that the beam minimum diameter decreases linearly with E_K. Thus, the diameters were plotted as a function of E_K and the results extrapolated to E_K = 9, 10 and 11 kV in Figure 22. The points at E_K = 5 and 6 kV are measured data points above 4 kV and show the onset of ion focussing. The presence of ions in the beam neutralized the space charge, and the beam collapsed to a smaller diameter than if the ions weren't present. Ion focussing depends strongly on the peak power density in the beam. At E_K = 4 kV tetrode #4 delivered a maximum of approximately 1 kW/mm^2. This value is the upper bound in power density which the current tungsten pinhole can withstand.

The extrapolation of diameters in Figure 22 yields no information about the beam shape at E_K = 9, 10 or 11 kV. The second method of determining the beam minimum diameter is an extrapolation of the entire waist profile. Knowing the overall gain in the system, the total current passing through the pinhole at selected points in the beam was computed for profiles taken at the waist. Since the total beam current varied according to the perveance law for different E_K's, so did the pinhole current for most points in the beam. Pinhole currents were computed at 0.005" increments across the beam for each waist profile corresponding to a unique E_K. The waist profile at E_K = 1.5 kV for tetrode #4, shown in Figure 23, displays these computed current values around the edge of the profile. These currents, raised to the 2/3 power, were plotted as a function of E_K in Figure 24. Each line represents the extrapolated

31
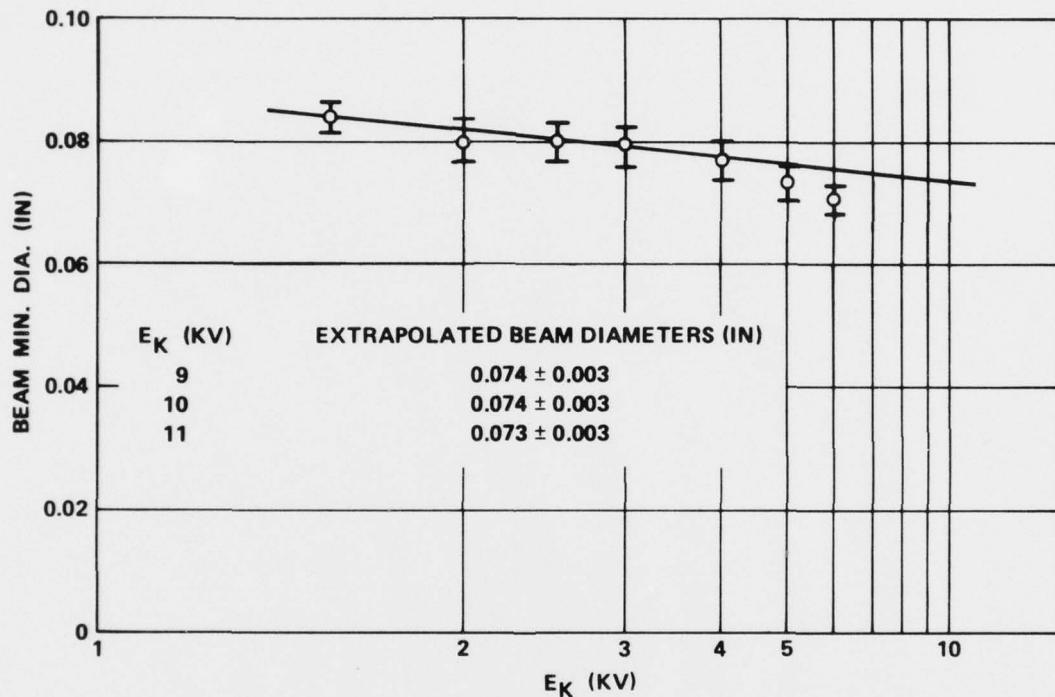
FIGURE 22   PULSE MODE BEAM MINIMUM DIAMETERS VS. E_k FROM
TETRODE #4 WITH E_f = 5.5V AND E_{g1}/E_{g2} = .61
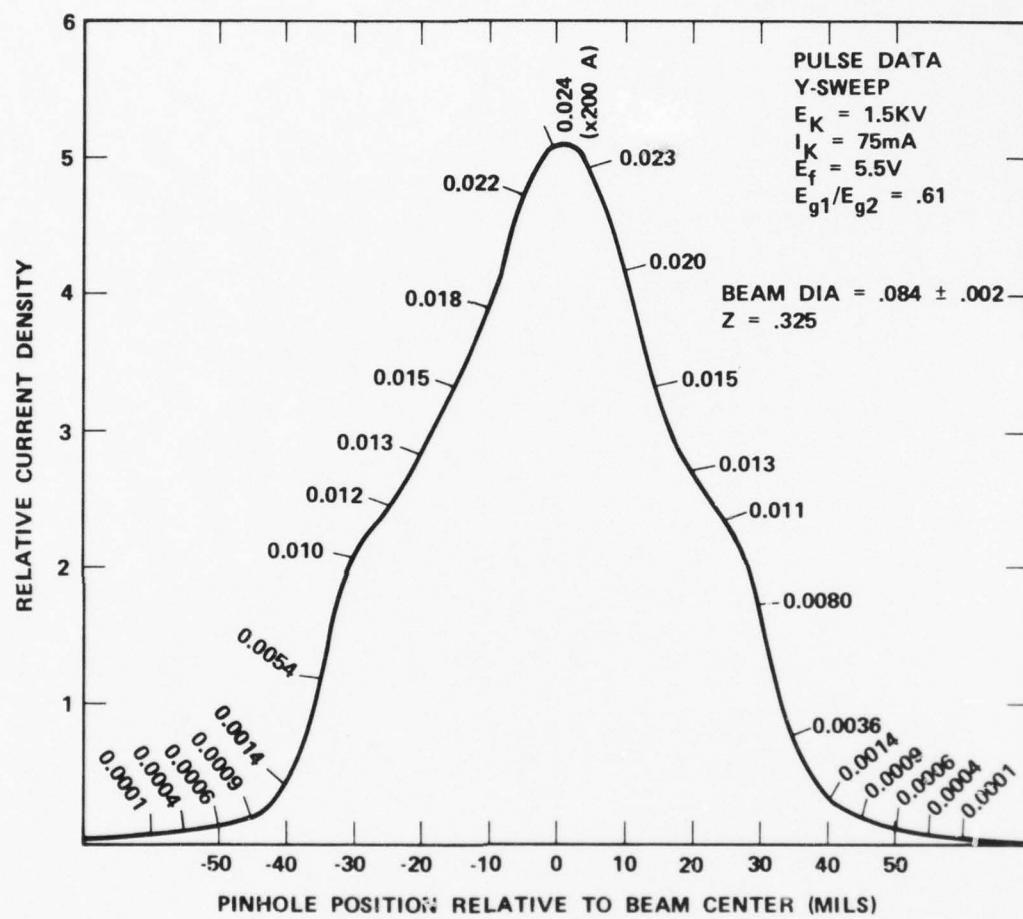
FIGURE 23   WAIST PROFILE FROM TETRODE #4 DISPLAYING
COMPUTED PINHOLE CURRENTS.
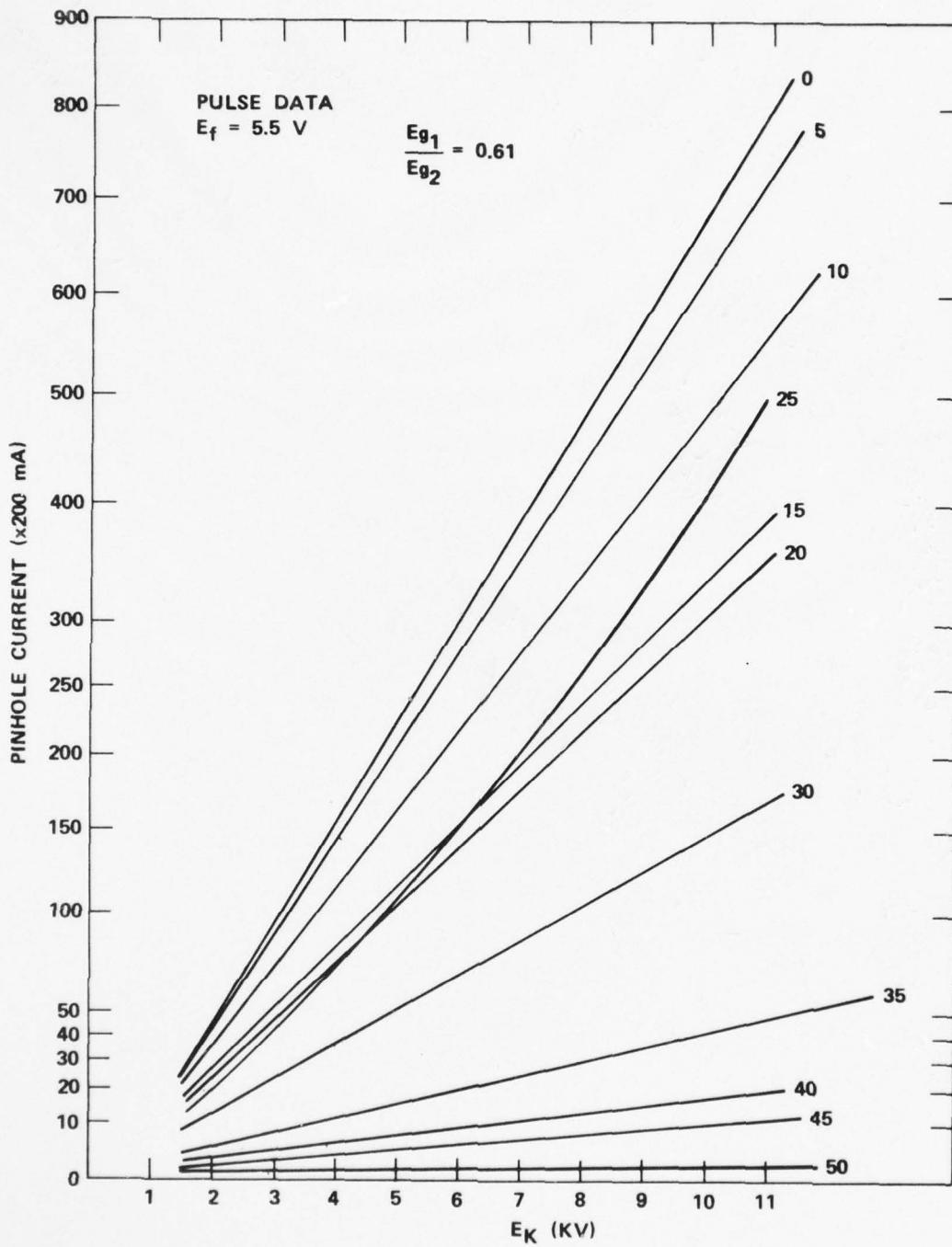
FIGURE 24   PINHOLE CURRENTS VS. E_k FROM TETRODE #4.

pinhole current versus E_K at a specific point in the beam. For example, the line marked "5" is the pinhole current extrapolation for the point 0.005" to the right of beam center. Note that all extrapolations are linear with the exception of the line marked "25". The profile in Figure 23 has current density "shoulders" at 0.025" from beam center. As E_K was increased with the perveance held constant, the shoulders became more pronounced. Figure 25 shows this change when E_K was increased to 4 kV. This change in profile shape causes the non-linear extrapolation of the "25" line. A similar set of extrapolations was made for points to the left of beam center. To obtain the beam diameters at E_K = 9, 10 and 11 kV, the above extrapolations were used to plot the waist profiles. The beam diameters were extracted from the extrapolated profiles in the same fashion as those diameters of tetrodes #2 and #3.

3.7 ANALYSIS OF TETRODE #4

Pulse mode data for tetrode #4 was taken under 3 sets of conditions with different combinations of grid drives and filament voltages. The gun was originally used on the 572H, S/N 250 tube with E_f = 5.5V and Eg_1/Eg_2 = 0.61. The first set of data was taken under these conditions. Figures 22 and 26 show the beam minimum diameters found by methods 1 and 2, respectively. Comparison of the diameters for corresponding values of E_K show percent differences no greater than 3%. The most obvious feature of the profiles in Figure 26 is the prominent shoulders on either side of beam center. Estimates of the amount of current in the shoulders range from 50 to 60% of the total beam current. The symmetry of these profiles indicates that misalignment of the grids is probably not responsible for the shoulders.

The effects of varying the filament voltage on the beam profile were not investigated on tetrodes #2 or #3. The second set of data on tetrode #4 was taken with Eg_1/Eg_2 = 0.61, with the filament voltage raised to 7.0V.
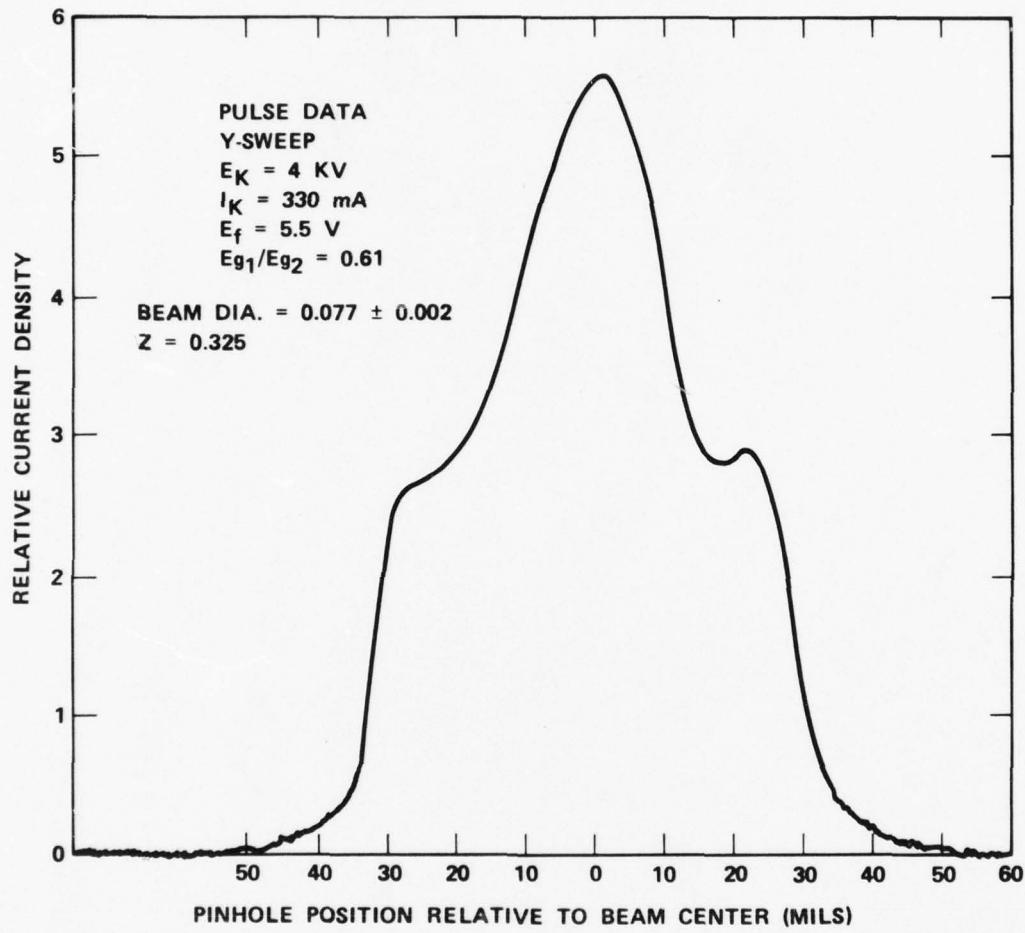
FIGURE 25   WAIST PROFILE FROM TETRODE #4 ILLUSTRATING BEAM SHOULDERS.
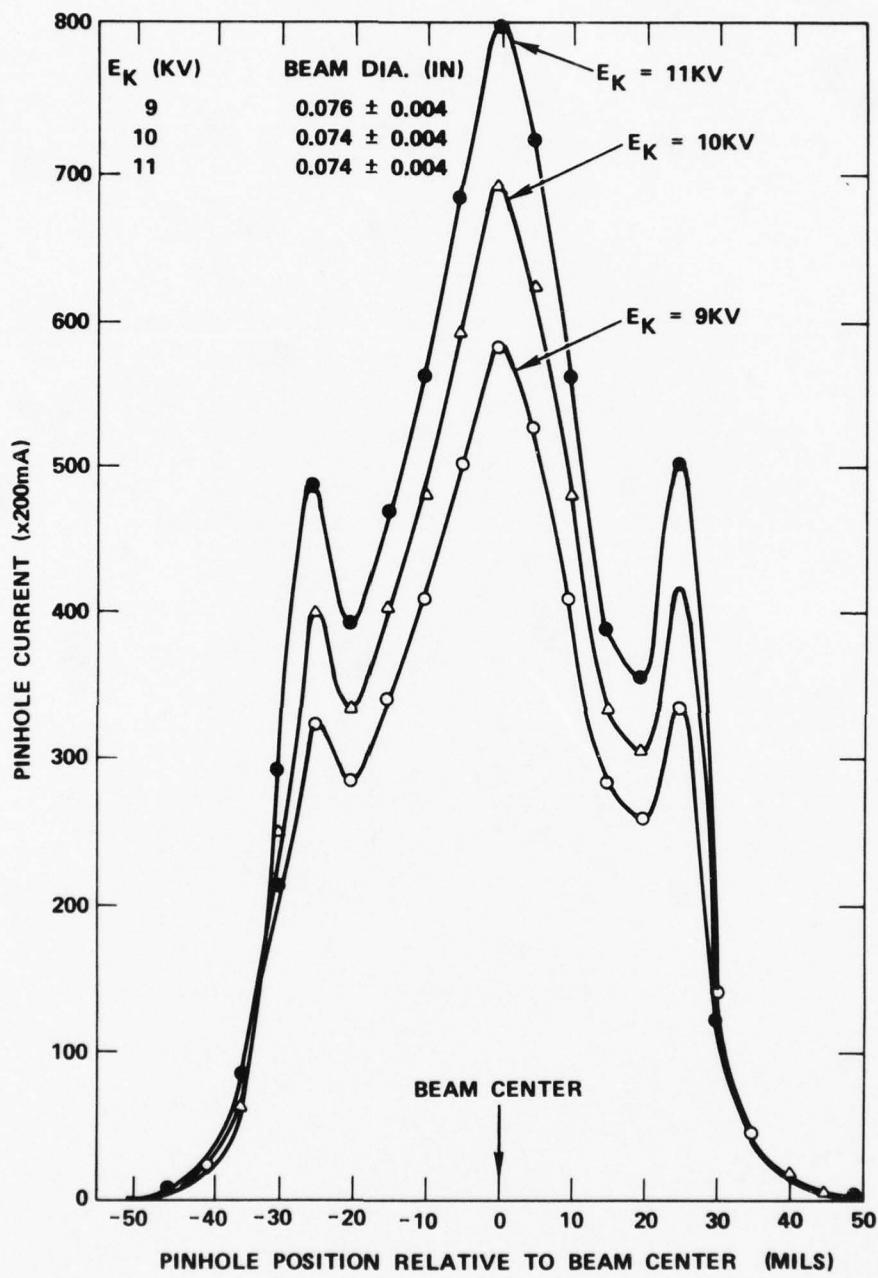
FIGURE 26   PULSE MODE BEAM PROFILE EXTRAPOLATIONS FROM
TETRODE #4 WITH E_f = 5.5V AND E_{g1}/E_{g2} = .61.

37

The beam minimum diameters are plotted versus E_K in Figure 27 and the profile extrapolations are shown in Figure 28. Comparing the corresponding extrapolated diameters shown in Figures 22 and 27 reveals a 5% increase in the diameter when the filament voltage was increased from 5.5V to 7.0V. Comparing the diameters found from the profiles in Figures 26 and 28 shows a 7% increase when E_f was increased. The increase in beam diameter is expected, since thermal spreading of the beam is more prevalent at higher filament voltages.

The third set of conditions for pulse mode data was $E_{g_1}/E_{g_2} = 0.45$ and $E_f = 5.5V$. The results are shown in Figures 29 and 30. The diameters were nearly identical to those observed with $E_{g_1}/E_{g_2} = 0.61$ and $E_f = 5.5V$. Thus, the change in E_{g_1}/E_{g_2} had little effect on the beam, contrary to the results from tetrode #2.

The CW mode data was taken with $E_{g_1} = -150V$ and $E_f = 5.5V$. The perveance was held constant at 0.32 μP for all values of E_K. Data was taken and analyzed in the same fashion as pulse mode data with the results shown in Figures 31 and 32.

An obvious difference between the pulse and CW mode profiles is the absence of shoulders in the CW profiles. Recall that in the CW mode the screen grid suppresses emission from the outer portion of the cathode. Consider a gun with only one grid, the screen grid. If the grid is pulsed with a positive voltage, it will draw current from the cathode. If the grid is pulsed with a voltage smaller than the "invisible" voltage, a hollow beam will be produced. A tetrode gun with both grids pulsed positively would produce a superposition of a hollow beam and a peaked beam. The pulse mode profile appears to fit that model.

38
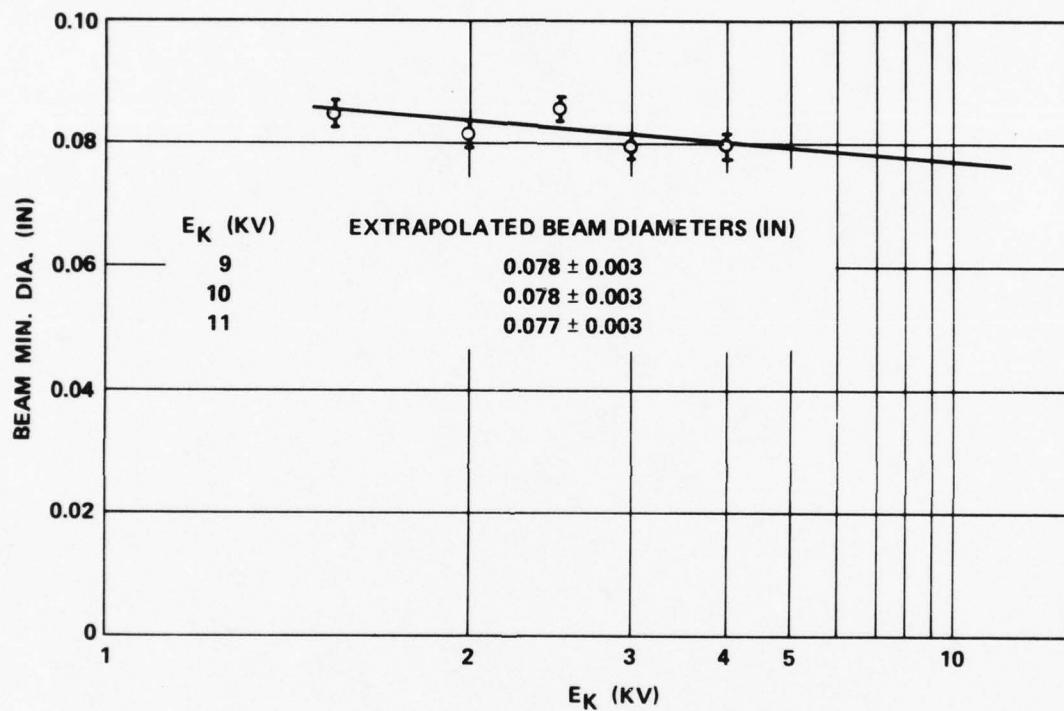
FIGURE 27   PULSE MODE BEAM MINIMUM DIAMETER VS. E_k FROM
TETRODE #4 WITH E_f = 7.0V AND E_{g1}/E_{g2} = .61
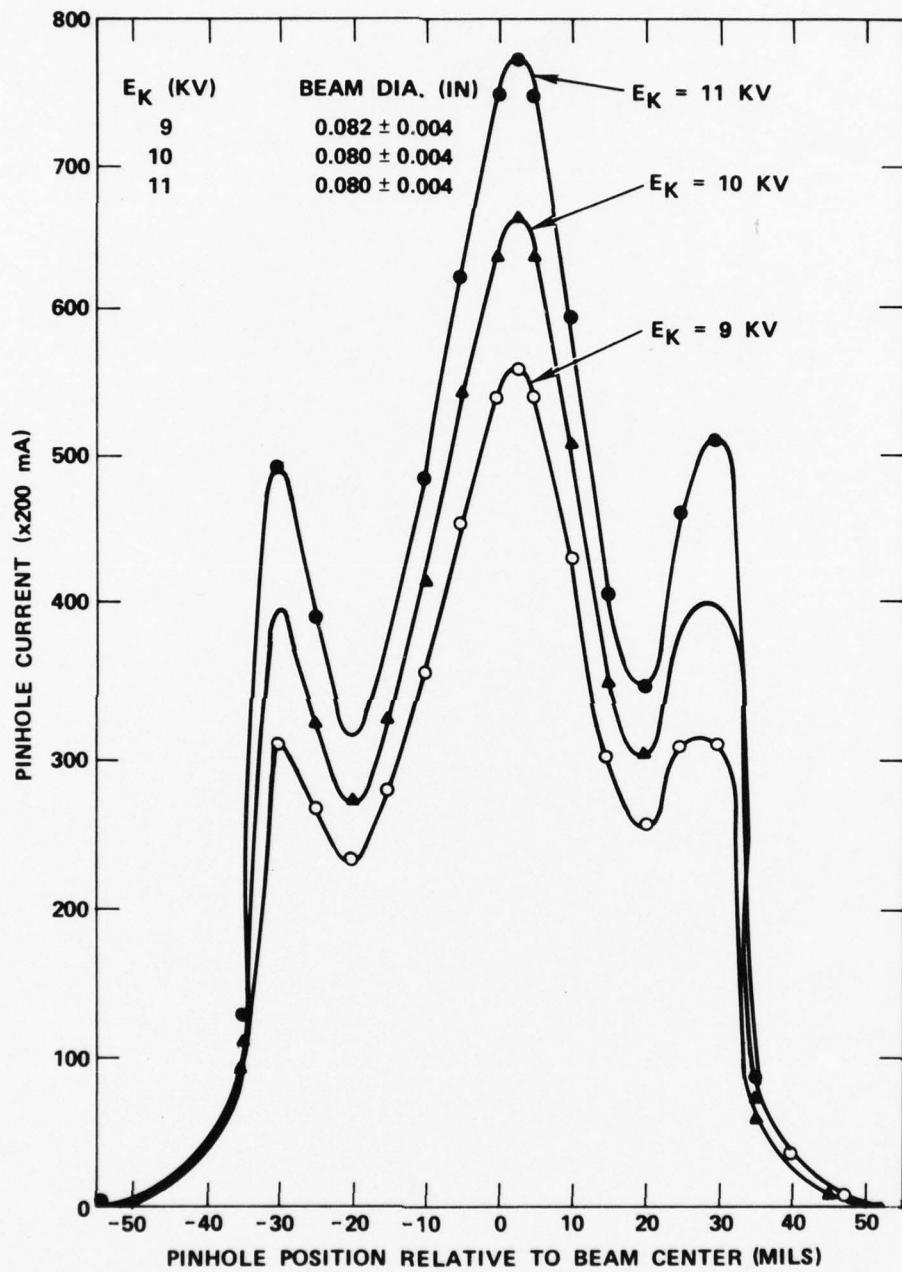
FIGURE 28   PULSE MODE BEAM PROFILE EXTRAPOLATIONS FROM
TETRODE #4 WITH E_f = 7.0V AND E_{g1}/E_{g2} = .61
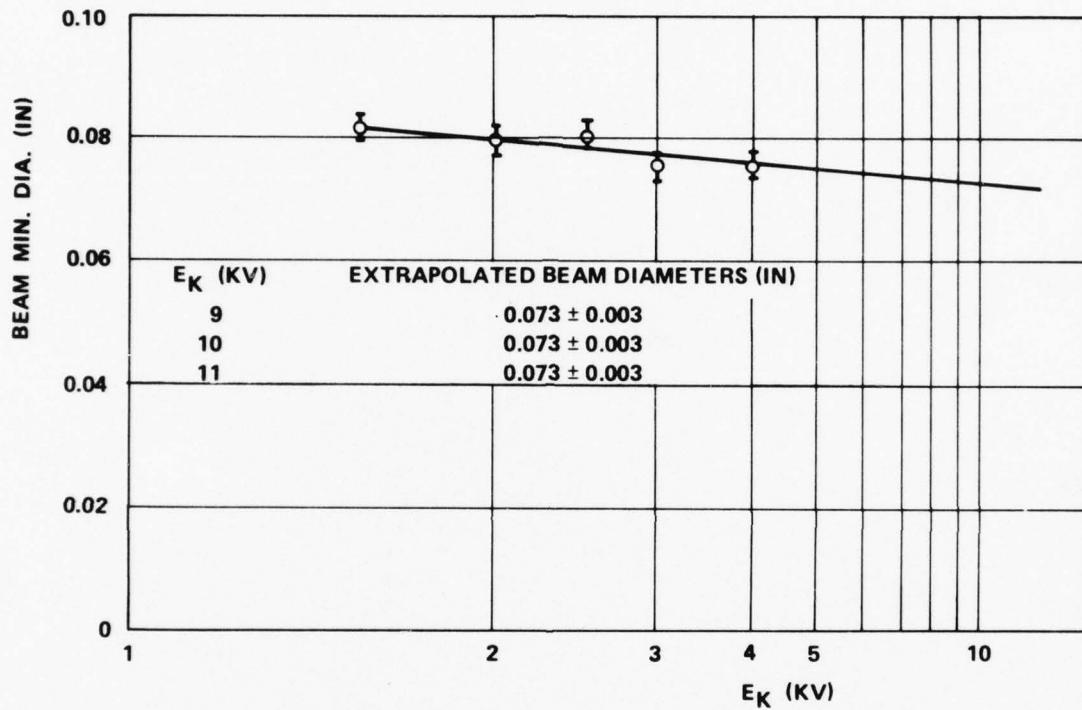
FIGURE 29   PULSE MODE BEAM MINIMUM DIAMETERS VS. E_k FROM
TETRODE #4 WITH E_f = 5.5V AND E_{g1}/E_{g2} = .45
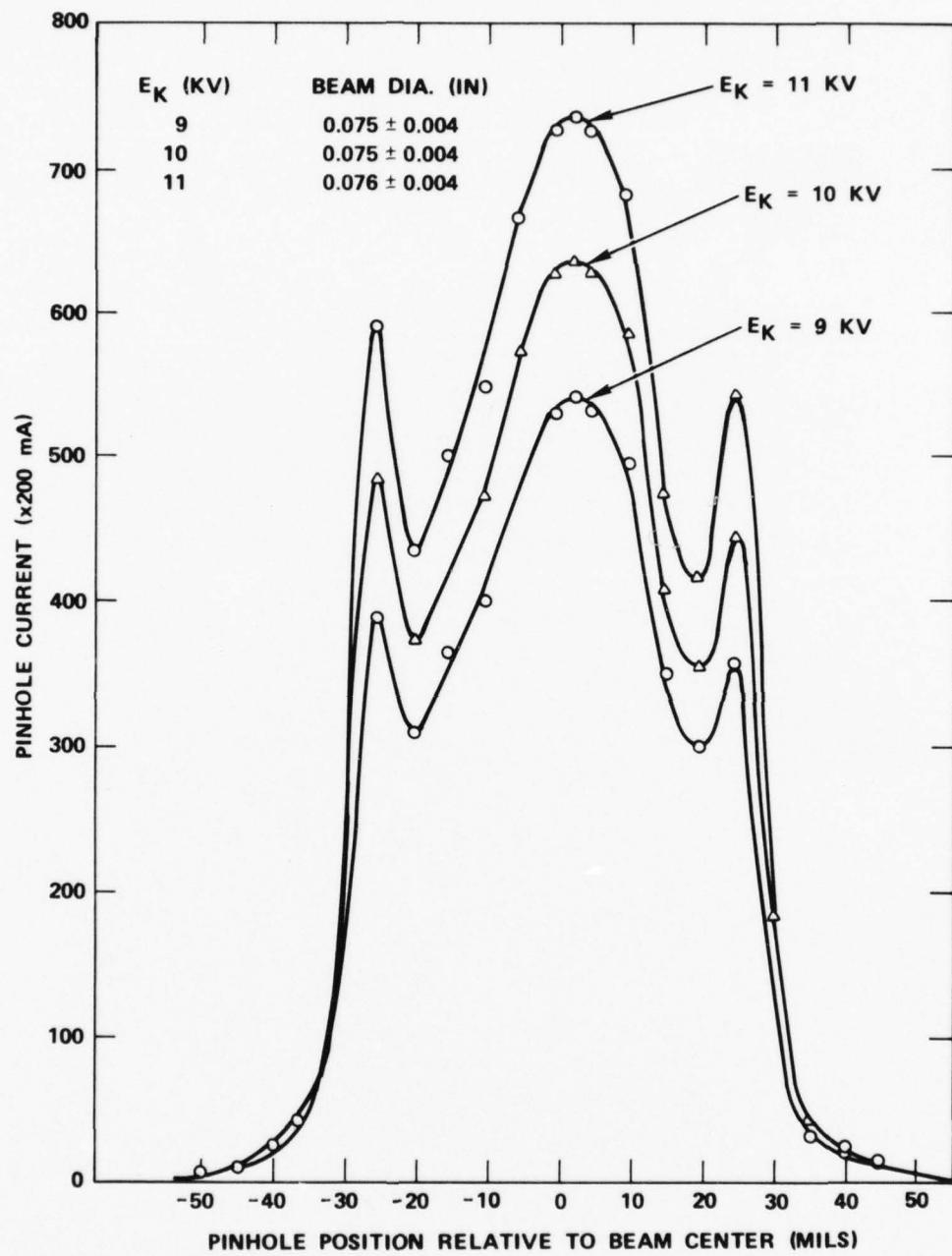
FIGURE 30   PULSE MODE BEAM PROFILE EXTRAPOLATIONS FROM
TETRODE #4 WITH E_f = 5.5V AND E_{g1}/E_{g2} = .45

G6402
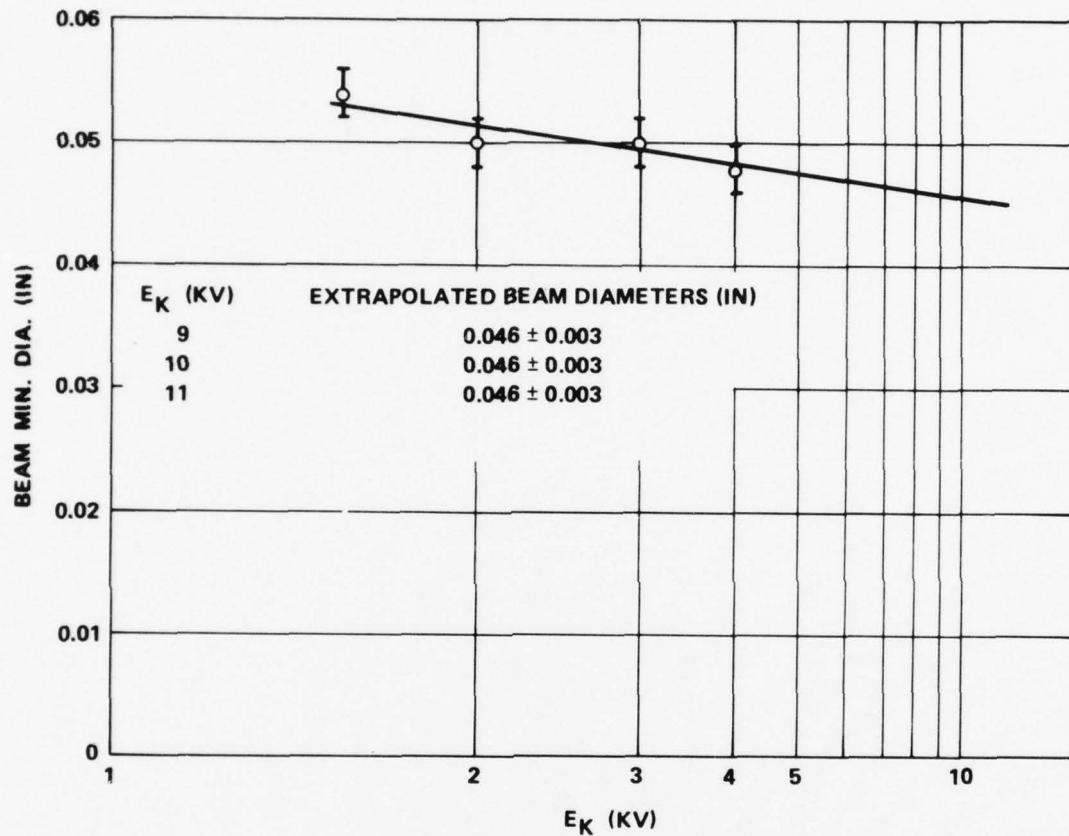
FIGURE 31   CW MODE BEAM MINIMUM DIAMETERS VS. E_k FROM
TETRODE #4 WITH E_f = 5.5V AND E_{g1} = -150V.

43
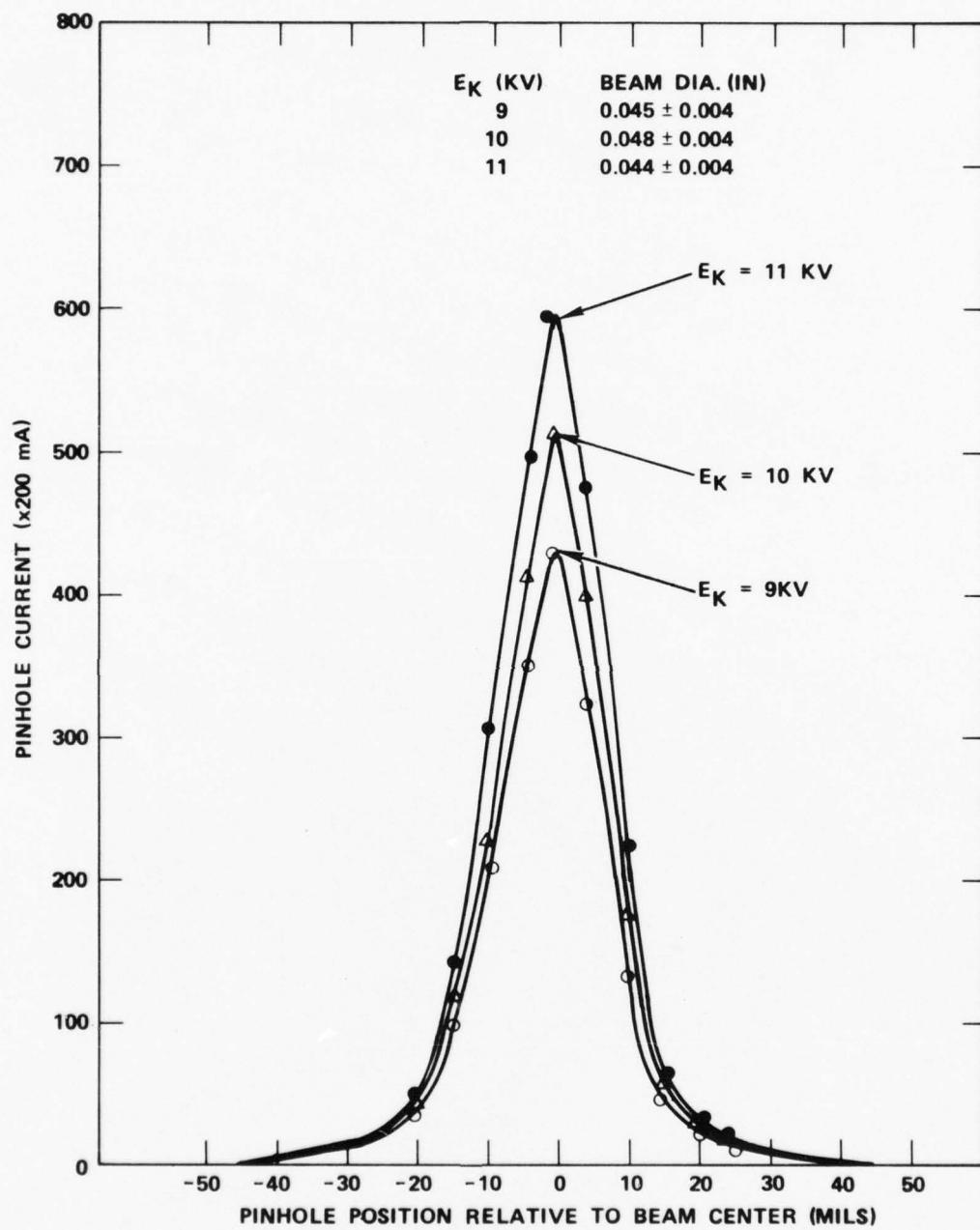
FIGURE 32   CW MODE BEAM PROFILE EXTRAPOLATIONS FROM
TETRODE #4 WITH E_f = 5.5V

3.8 ANALYSIS OF TRIODE #5

The last gun tested was triode #5 illustrated in Figure 33. Notice
that only one modulating grid exists in contrast to the tetrode gun.
Consequently, in the triode gun the entire cathode surface emits in both
modes. Like the tetrode gun the CW mode delivers a beam current of
300 mA, and the pulse mode delivers 1.2A. Both modes operate at $E_K = 9$,
10 or 11 kV.

Data was taken in the same fashion as that for tetrode #4. Beam minimum
diameters in the pulse mode are shown in Figures 34 and 35. Notice the
asymmetry in the extrapolated profiles of Figure 35. The pulse mode
beam minimum position was constant at 0.325" from the cathode center.

The corresponding results in the CW mode are shown in Figures 36 and 37.
Notice that for all values of cathode voltage, E_K, the diameters are
smaller than those found in the pulse mode. Even though the entire
cathode surface emits in both modes, the CW mode contains less space
charge and the beam collapses more than in the pulse mode. Notice also
that the extrapolated profiles are relatively symmetric and peaked.
These extrapolations are at the beam waist. For all $E_K \leq 4$ kV the
beam profiles were consistently asymmetric at all axial positions other
than the waist. An example of this asymmetry is shown in Figure 38.
This apparent asymmetry existing in both modes was probably due to a
crooked control grid. The beam minimum position for the CW mode was
located at 0.365", 0.040" farther from the cathode than in the pulse
mode.

Using a triode gun in a dual mode system has one drawback compared to a
tetrode gun. For a triode gun operating at a fixed E_K, a unique
"invisible" potential exists as a grid voltage. Since different grid
voltages are used in the CW and pulse modes, one of those modes invari-
ably has a non-laminar beam; both modes cannot have invisible grid
voltages.

45

G6404
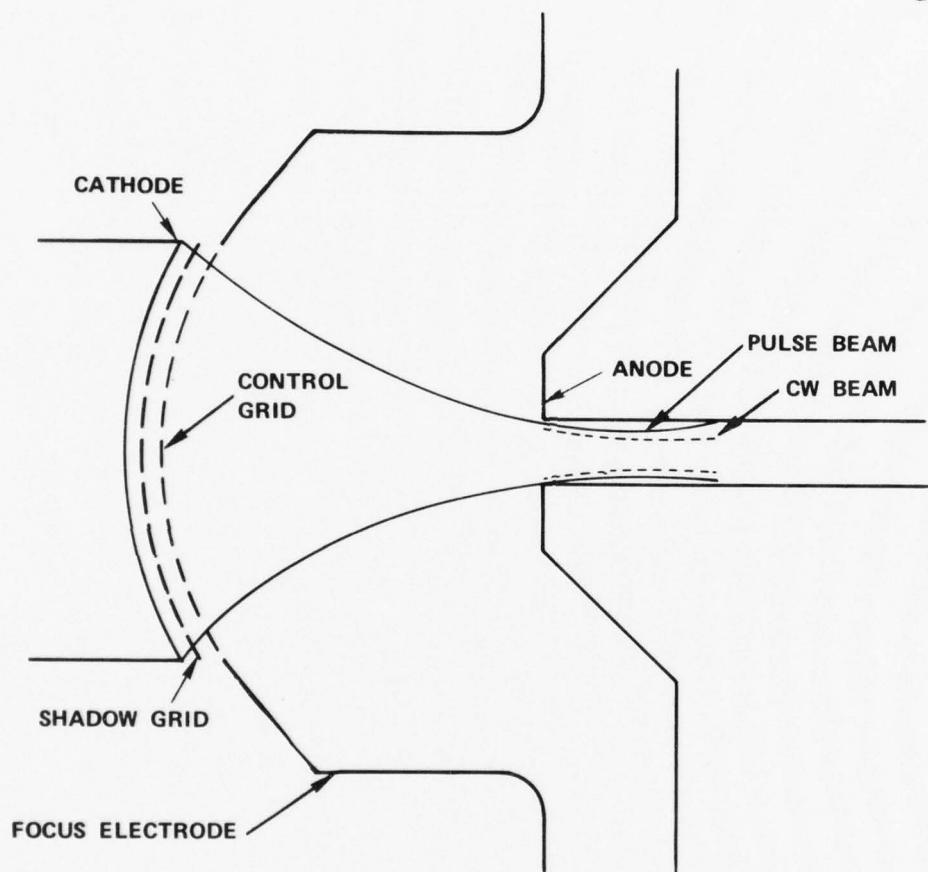
FIGURE 33   ELECTRODE CONFIGURATION OF A SHADOW GRIDDED TRIODE GUN

0.14

0.12

0.10

BEAM MIN. DIA. (IN)

0.08

0.06

E_K (KV)	EXTRAPOLATED BEAM DIAMETER (IN)
9	0.066 ± 0.001
10	0.064 ± 0.002
11	0.063 ± 0.002

0.04

0.02

0

1.0   2.0   3.0   4.0 5.0   10.0

E_K (KV)
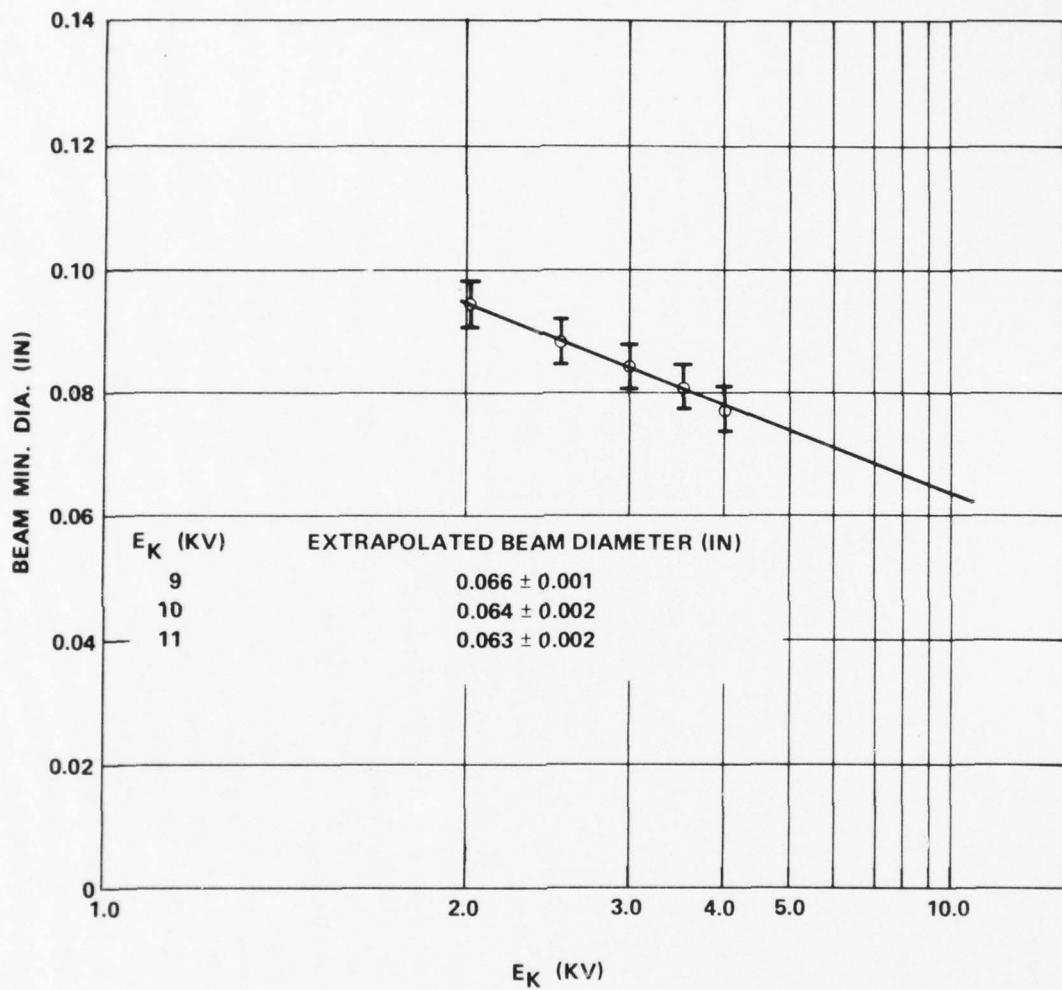
FIGURE 34   PULSE MODE BEAM MINIMUM DIAMETERS VS. E_k FROM
TRIODE #5 WITH E_f = 7.0V
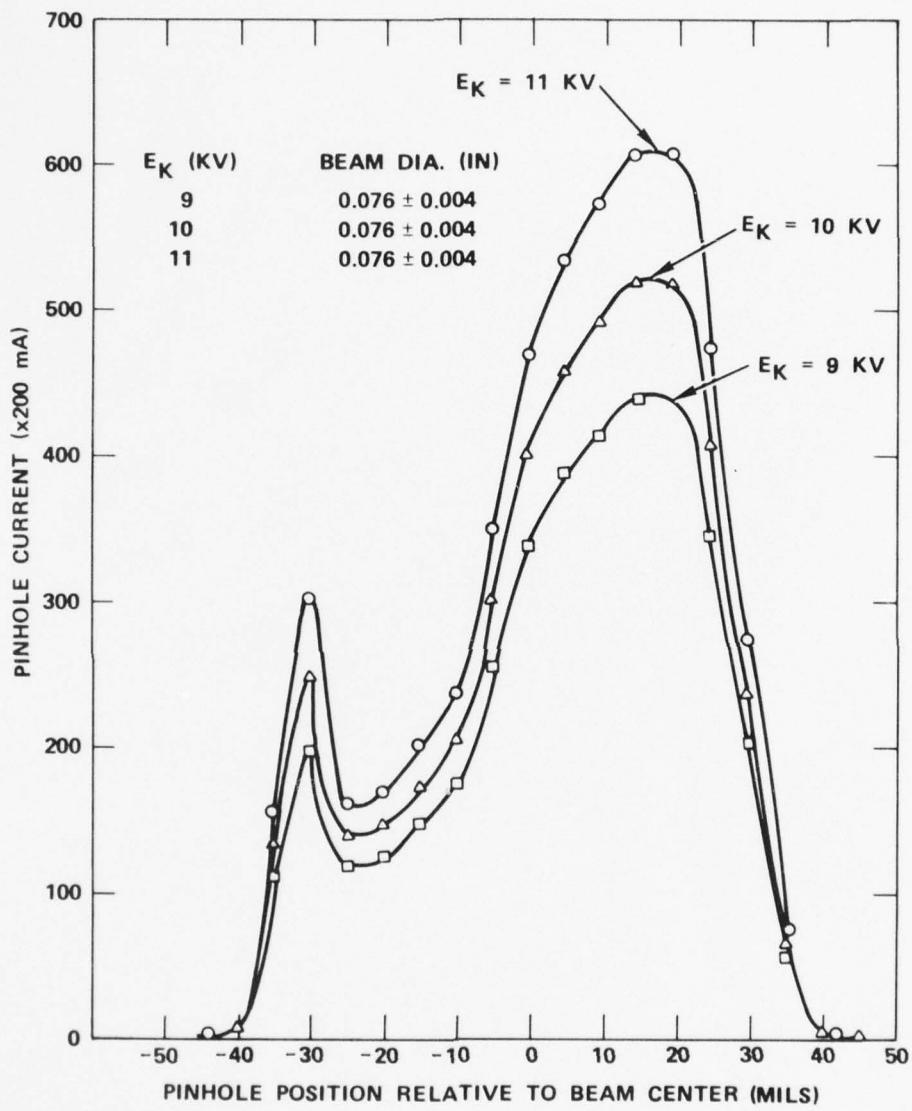
FIGURE 35   PULSE MODE BEAM PROFILE EXTRAPOLATIONS FROM
TRIODE #5 WITH E_f = 7.0V
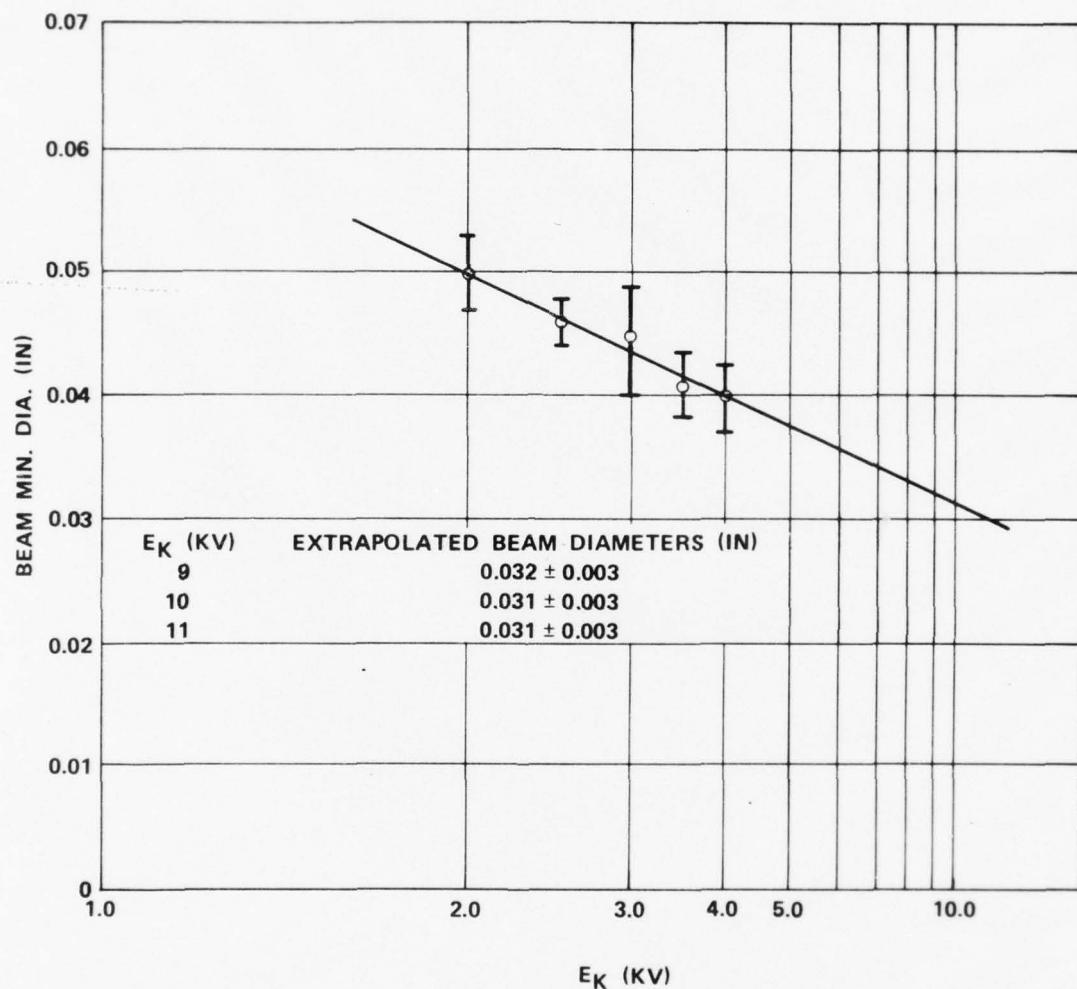
FIGURE 36   CW MODE BEAM MINIMUM DIAMETERS VS. E_k FROM
TRIODE #5 WITH E_f = 7.0V

G6408
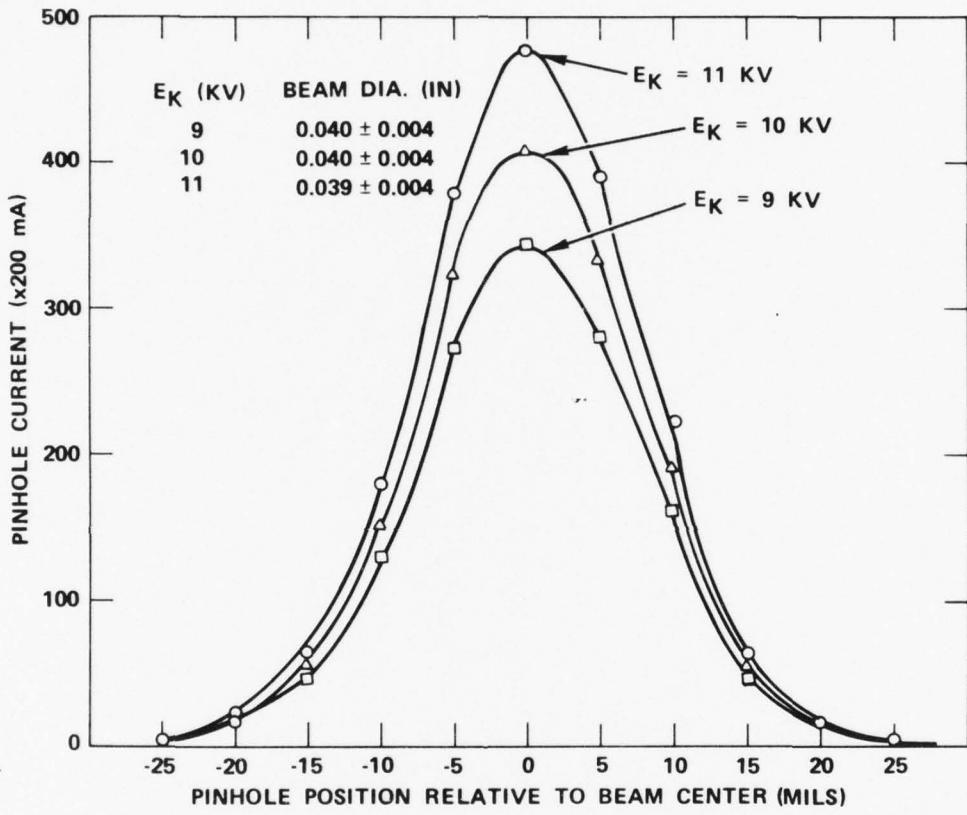
FIGURE 37   CW MODE BEAM PROFILE EXTRAPOLATIONS FROM
TRIODE #5 WITH E_f = 7.0V
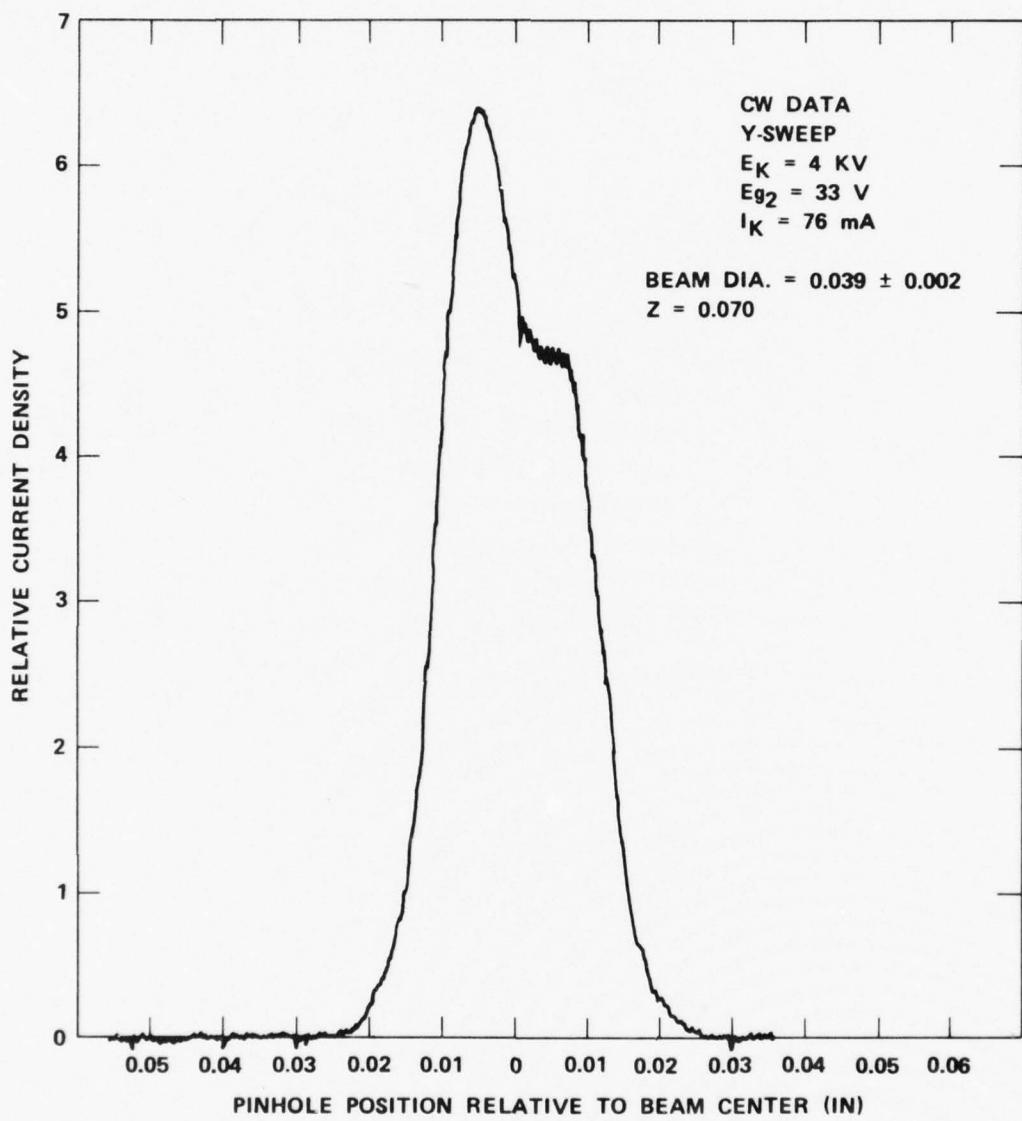
FIGURE 38   CURRENT DENSITY PROFILE FROM TRIODE #5

3.9 COMPARISON OF GUNS

Tables 2 and 3 summarize the beam minimum diameter and positions for all
four guns. The diameters in Table 2 are normalized to the design perve-
ances (1.2 μP for the pulse mode, and 0.3 μP for the CW mode) and to
E_f = 6.3V. Notice that among the tetrode guns, #4 showed no variation
in diameter as Eg_1/Eg_2 varied, whereas #2 and #3 did. Also, the diam-
eters of #4 showed little dependence upon E_K. The beam diameters of
the triode gun in the CW mode are most similar to those of the vaneless
tetrode #3. This is expected, because the electrode configuration of a
triode gun more closely resembles the vaneless tetrode than the conven-
tional tetrode.

Since the data from the first two guns was taken at E_K = 9, 10 and 11 kV,
and the last two were analyzed by extrapolations from lower E_K's, it is
hazardous to compare quantitatively their performance. However, the
profile shapes varied radically between the two tetrode guns. There
was also much evidence of misaligned grids. Finally, the influence of
grid voltage on beam laminarity was clearly demonstrated.

TABLE 2

NORMALIZED BEAM MINIMUM DIAMETERS (IN)

$\dfrac{Eg_1}{Eg_2}$	Tetrode #2 $E_k =$			Tetrode #3 (Vaneless) $E_k =$			Tetrode #4 $E_k =$		
	9 kV	10 kV	11 kV	9 kV	10 kV	11 kV	9 kV	10 kV	11 kV
.45	-	-	-	-	-	-	.077 ±.004	.077 ±.004	.076 ±.004
.50	.066 ±.006	.094 ±.004	.078 ±.006	.047 ±.003	.052 ±.002	.057 ±.002	-	-	-
.61	-	-	-	-	-	-	.077 ±.004	.077 ±.004	.076 ±.004
.75	.084 ±.008	.100 ±.004	.114 ±.004	.045 ±.002	.054 ±.002	.059 ±.002	-	-	-
CW Mode	.042 ±.002	.047 ±.002	.061 ±.002	.024 ±.002	.032 ±.002	.041 ±.002	.049 ±.004	.050 ±.004	.047 ±.004

Mode	Triode #5 $E_k =$		
	9 kV	10 kV	11 kV
Pulse	.068 ±.004	.068 ±.004	.068 ±.004
CW	.033 ±.004	.034 ±.004	.033 ±.004

TABLE 3

BEAM MINIMUM POSITIONS
(INCHES FROM CATHODE CENTER)

Gun	Pulse Mode	CW Mode
Tetrode #2	.250 - .330	.290 - .320
Tetrode #3	.335	.335
Tetrode #4	.325	.325
Triode #5	.335	.365

4.0   SANDWICH GRID FABRICATION METHOD

4.1   SANDWICH GRID CONCEPT

The essential feature of the "sandwich" method of fabricating grids is
that the <u>blank</u> grid discs are permanently attached to a supporting iso-
lator while being separated by spacer discs of suitable thickness and
<u>then</u> the dome formed and the grid pattern machined into the "sandwich".
The spacer material is then chemically removed leaving a finished multi-
ple grid assembly.   The thickness of the spacer material determines the
final spacing between the grids.   The simultaneous forming gives
extremely accurate dome concentricity.   Finally, the simultaneous machin-
ing guarantees very accurate grid pattern concentricity and azimuthal
alignment.   Figures 39, 40 and 41 show cross-sectional sketches of a
brazed, formed, and final assembly.

4.2   DEVELOPMENT OF SANDWICH GRID ASSEMBLY TECHNIQUE

There were several problems encountered while trying to produce a func-
tional sandwich grid assembly.   Most were relatively simple manufactur-
ing problems which had obvious solutions.   The problem areas included
tooling, assembly processing, and lead attachment.   Following is a dis-
cussion of the major fabrication operations and the problems and solu-
tions relating to them.

4.2.1   Brazing Operations

The shadow grid disc and control grid disc are made of drawing grade
molybdenum rhenium alloy and the cylinders which attach to these discs
are molybdenum.   Initially, it was attempted to assemble the cup assem-
blies using Nioro braze material.   Even though the parts were cleaned
in a dry hydrogen furnace first, wetting of the braze material was poor
and the braze joints were marginal.   This braze operation was used in

G6410
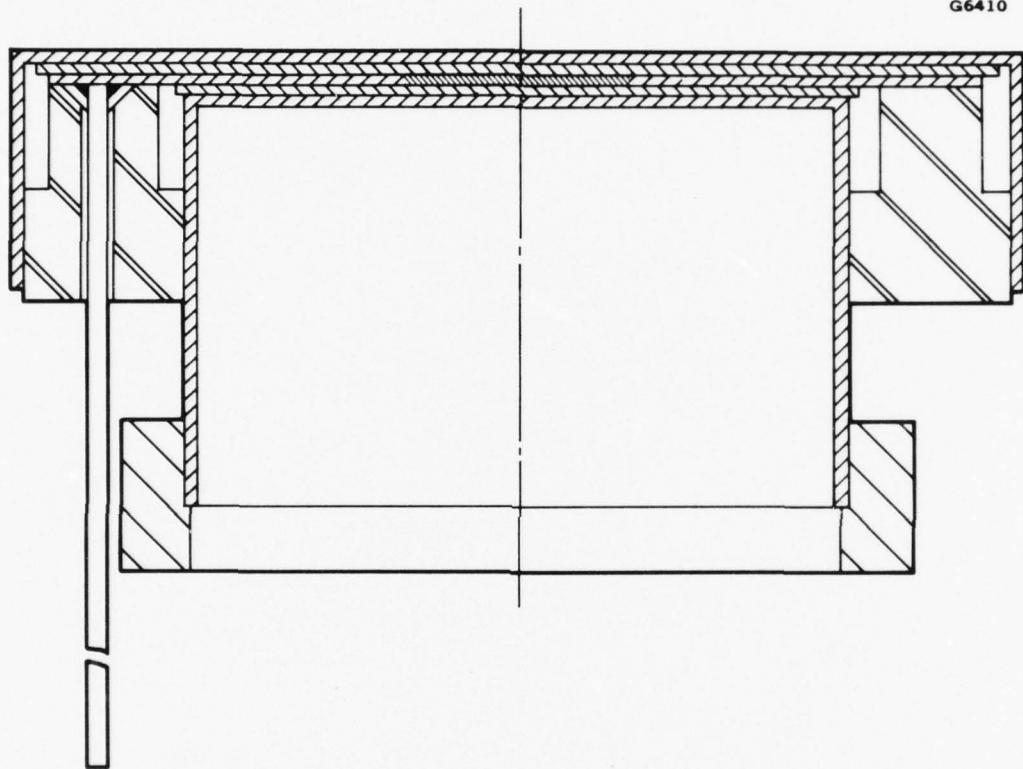
FIGURE 39   SANDWICH GRID ASSEMBLY AS BRAZED

G6411
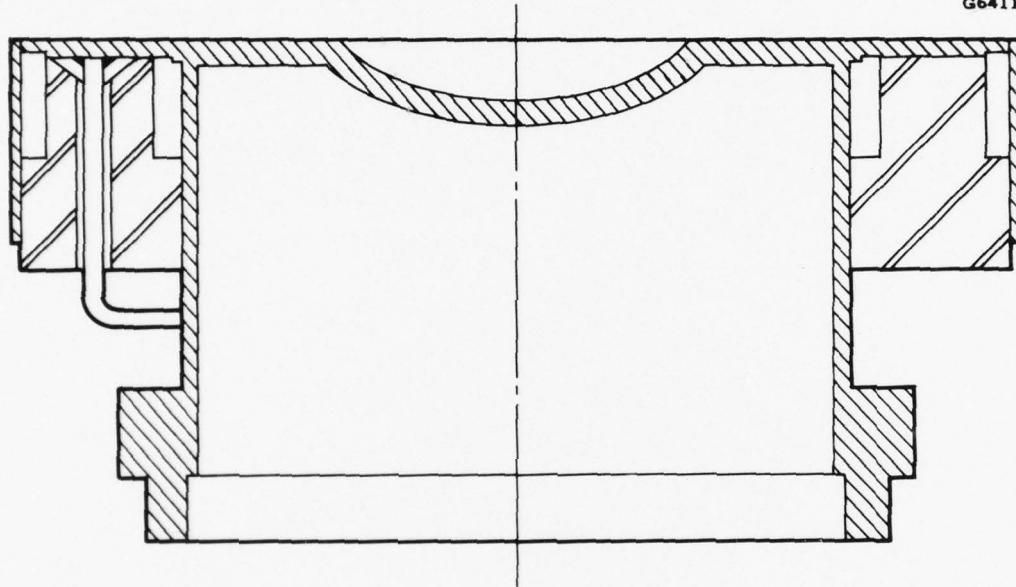
FIGURE 40   SANDWICH GRID ASSEMBLY AFTER FORMING AND
PRIOR TO MACHINING AND SPACER REMOVAL
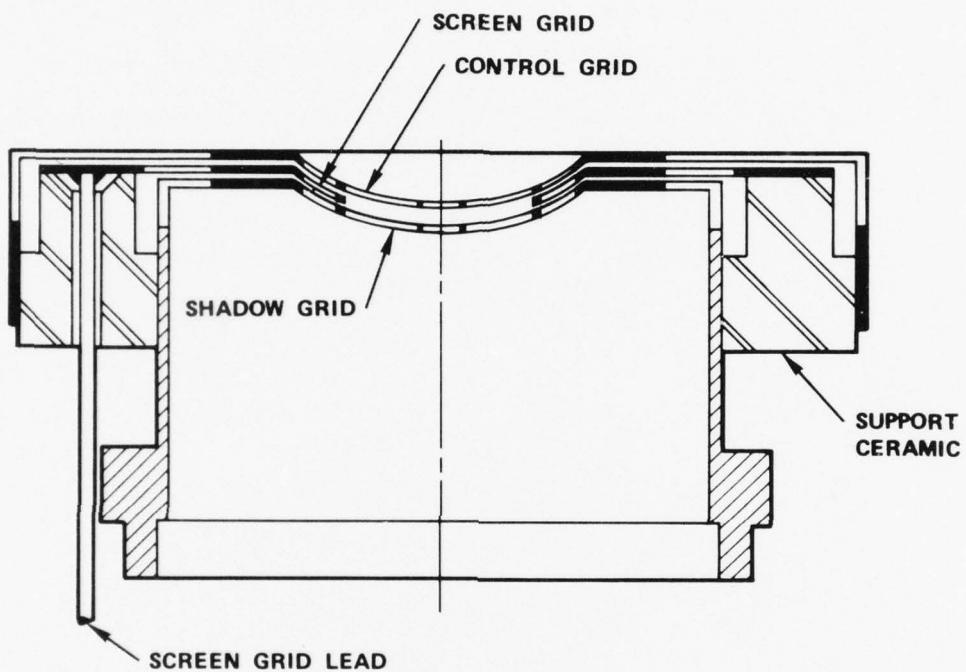
FIGURE 41   FINISHED SANDWICH GRID ASSEMBLY

conjunction with a Nicoro 80 braze of the two cups and screen grid to
the support ceramic. The remedy for the poor braze joints was to nickel
plate all of the molybdenum and molybdenum-rhenium piece parts (includ-
ing the lead) and use copper/gold alloy braze materials in wet hydrogen
braze operations. With these changes, the braze flow was quite good.
The nickel plating, however, did show some problems with "blistering"
after brazing. It is also an extra variable to be considered in the
operation which removes the spacers chemically. In the future, it is
probable that the plating will be confined to just the braze joint areas.
Another problem encountered was the brazing of the steel spacer discs
to the grid discs. This results in inaccurate spacing control and pro-
motes rupturing of the sandwich during the forming operation. The first
attempt at preventing this brazing was to black oxide coat the carbon
steel spacers. This proved to be only marginally effective. Next
stainless steel spacers which were "greened" in a wet hydrogen furnace
were tried. This eliminated the braze flow problem--but did create a
spacer removal problem (the stainless steel is attached by acid less
rapidly than carbon steel). The final solution was to chrome plate
carbon steel spacers and "green" them. This solved the problems.

The final problem encountered in the brazing operation was that of lead
attachment to the screen grid. In spite of coating the end of the lead
where it touches the screen grid with braze powder, numerous assemblies
had open leads. Figure 42 shows a sketch of what is felt to be the
problem. The remedy is shown in Figure 43. The countersink is not
metallized so it cannot draw braze material from the desired joint. In
addition, the lead is wired to the braze fixture to make sure it doesn't
lift up during the braze operation. Finally, a braze joint between the
lead and ceramic was added on the side of the ceramic opposite the
screen grid. This not only eliminates strains on the lead to screen
grid joint but also seals off the hole in the ceramic so acid can't be
trapped there after the spacer removal operation. These modifications
have resulted in good lead attachment.

PROBLEM – OPEN SCREEN GRID LEAD

CAUSE – LEAD NOT TOUCHING GRID BRAZE MATERIAL DURING FIXTURING

BEFORE BRAZE

AFTER BRAZE
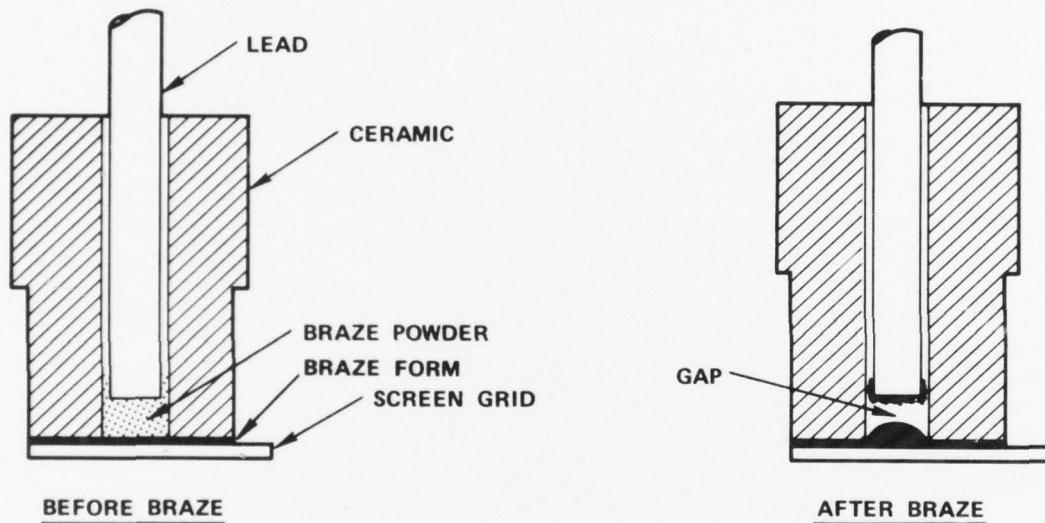
FIGURE 42   SANDWICH GRID LEAD ATTACHMENT PROBLEM

G6414

LEAD
BRAZE WIRE
METALLIZATION
CERAMIC

COUNTERSINK

BRAZE POWDER
BRAZE FORM
SCREEN GRID

BEFORE BRAZE

BRAZE JOINT

AFTER BRAZE
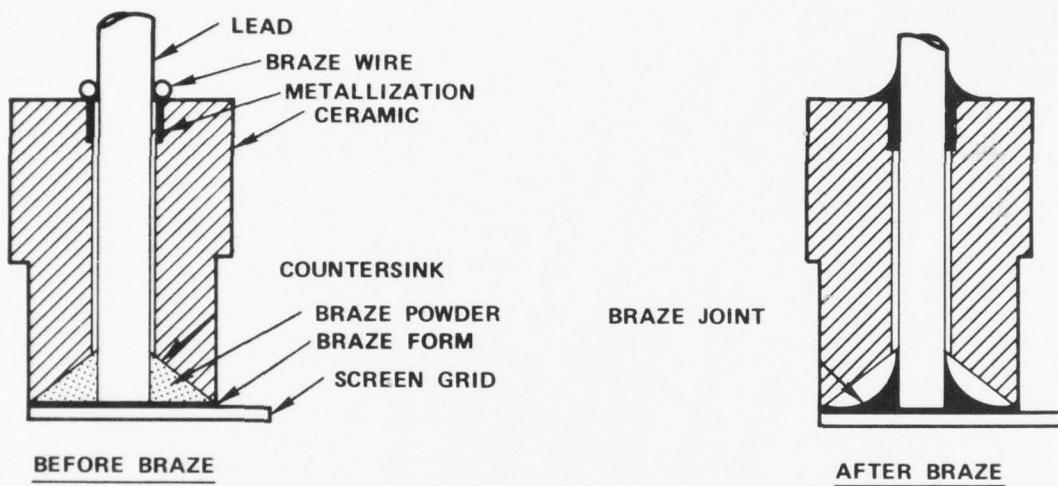
FIGURE 43   SANDWICH GRID LEAD ATTACHMENT

61

4.2.2 Forming Operation

The desired result of this operation is to produce a spherical radius in
the center of the sandwich (see Figure 44). Ideally, this "dome" should
have a height (on the convex side) equal to the female die depth and the
sandwich should be fully compacted (i.e., spring-back of the sandwich
materials should not be present). Also, the assembly should be stress
relieved to reduce temperature dependent dimensional changes. Through
a series of tests made on assemblies formed with various forces and all
at room temperature it was concluded that temperature setting the assem-
bly (while still in the forming die) in a furnace was necessary. It
appeared that most of the springback at room temperature was due to the
steel spacer material since the dome height was correct but the sandwich
thickness was on the order of 0.002 inches more than optimal. A series
of experiments resulted in a forming method which gives near optimal
results. The assembly is first pre-formed at room temperature with a
force high enough to fully compact and form the assembly (several hundred
pounds). The force is then reduced about 20% and the assembly and die
fired near 1000°C for about half an hour. The pressure reduction is
necessary to prevent diffusion bonding at some of the tooling interfaces
and tooling to assembly interfaces. With this method dome height is
within about 0.0002 inches of the die depth and the sandwich thickness
is within about 0.0003 inches of optimal (0.016 inches). In addition,
these dimensions from one assembly to the next seem to be repeatable to
within ±0.0001 inches or better. There were many tooling changes
required before the forming operation could be adequately performed.
This included configuration changes, material changes, and processing
changes. For example, all interfaces where diffusion bonding might
occur have at least one of the surfaces oxidized (chromizing was used
on the molybdenum pieces).

Another change was to add a relief chamfer on the O.D. of the female die
to prevent the rupturing of the shadow grid disc to cylinder braze. The

62

G6415

MALE DIE

SANDWICH THICKNESS

DOME HEIGHT

DIE DEPTH

FEMALE DIE
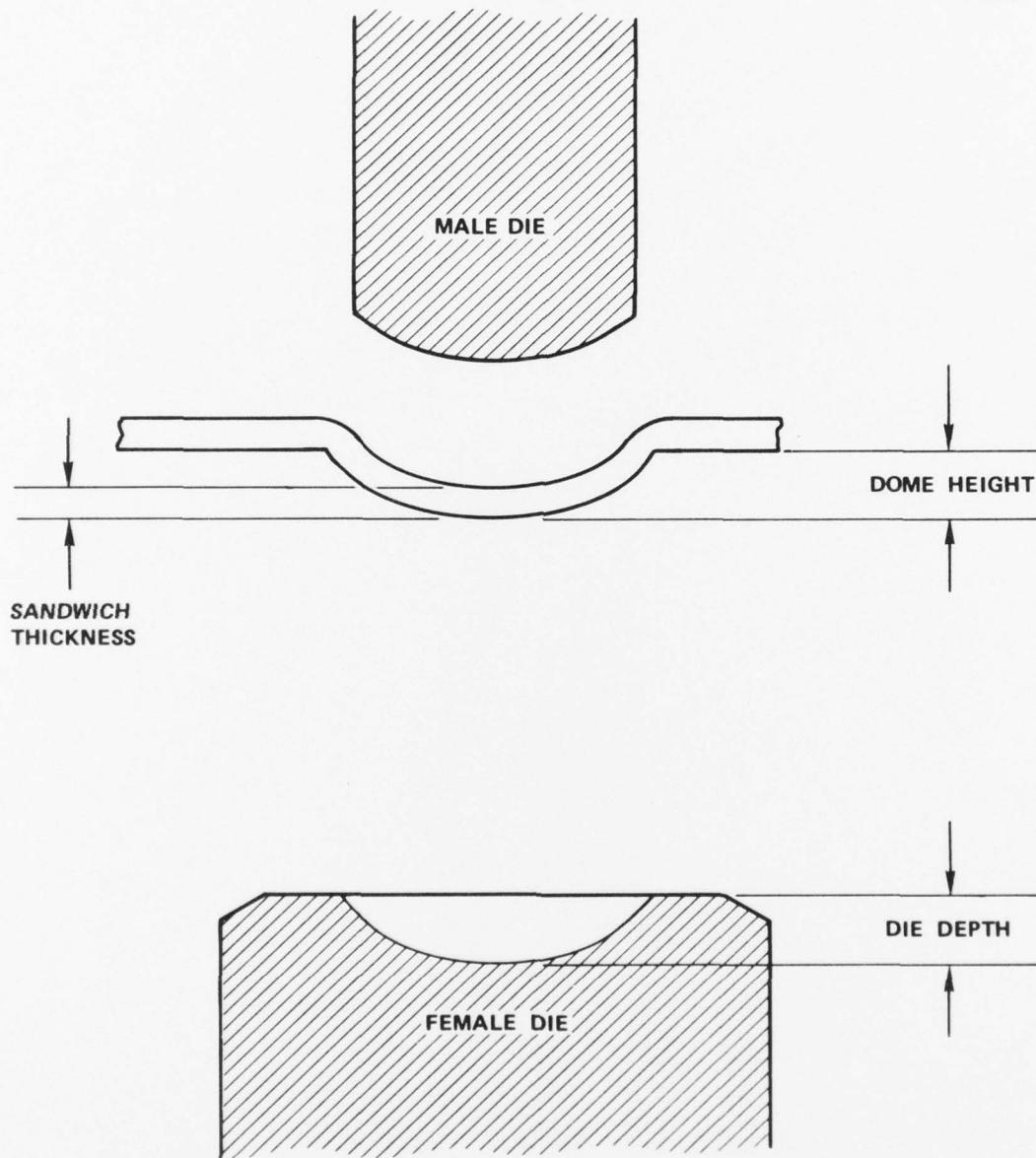
FIGURE 44 SANDWICH FORMING DIMENSIONS

forming tooling is still not optimal in that there is more assembly labor and expertise required than is desired, and the tooling requires a substantial amount of maintenance (mostly re-oxidizing of tool pieces) These problems, however, do not prevent obtaining correctly formed assemblies and might be the subject of some future effort in cost reduction.

4.2.3 Machining Operation

A two-step electrical discharge machining operation was utilized to produce the grid and slot pattern shown in Figure 45. First the grid pattern is machined with a vane width of about 0.002". During this operation there were two factors which substantially reduced the yield. The biggest factor was the non-concentricity of the machining tool with the inside diameter of the screen grid. This results in the annular ring of the screen grid being incomplete leaving only cantilevered radial vanes on one side of the grid. This problem was reduced somewhat by making the inside diameter of the blank screen grid disc a few mils smaller. Hopefully, a better means for aligning the screen grid with the machining tooling will be found to improve this yield. The use of photoetched piece parts may help in this area (tighter tolerance control). The second yield factor was the occasional separation of the grid sandwich layers during the machining operation. It is suspected that this was due to pressure created by the fluid used to flush the assembly during machining. A reduction in this fluid pressure seemed to reduce the problem, however, not enough assemblies have been machined to verify this as being the problem.

The second machining step produces the outer radial slots which expose the inner surfaces of the support ceramic. These facilitate the chemical removal of the steel spacers. They also allow for easier flushing and rinsing out of the residual acid used for spacer removal.

64

G6416

GRID VANES
0.003 MAX
0.002 MIN
32 PL

0.23 DIA

0.6 DIA

0.030 WIDE FLUSHING SLOT
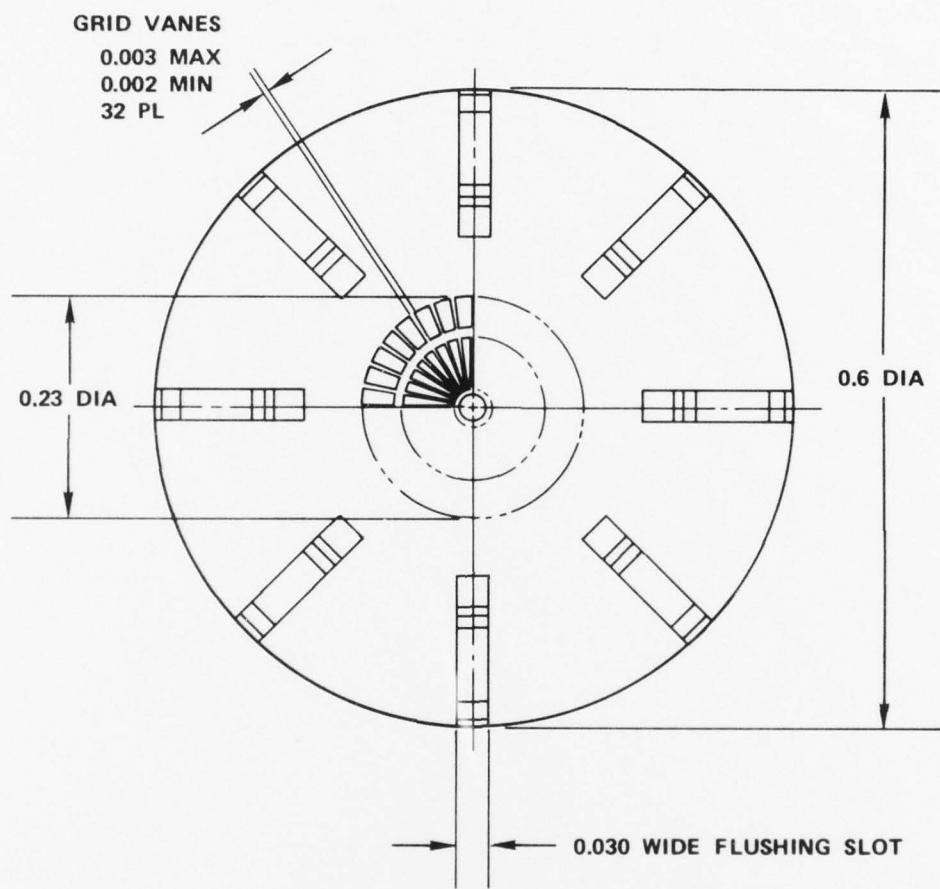
FIGURE 45   TOP VIEW OF MACHINED SANDWICH GRID

65

4.2.4 Spacer Removal Operation

The aim of this process is to chemically remove the iron spacers without attacking any other materials of the assembly and to leave no permanent contamination which would cause loss of electrical isolation between the grids or be a source of poison to the cathode. Most of the original etching was done with a 50% dilute solution of H_2SO_4 heated to about 80°C. To expedite the etching process, teflon fixturing was made to allow the acid to be pumped through the assembly. It was found that the alumina ceramic was being attached by the acid leaving black carbonaceous surface deposits. This has been eliminated by changing to HCL which also seems to leave a cleaner looking assembly overall.

4.2.5 Assemblies Fabricated

Through all the trial and error required for this development only a few assemblies made it to the etching operation in satisfactory condition. Figures 46, 47 and 48 are photo micrographs of one assembly after machining and prior to spacer removal. Figures 49 and 50 are photographs of the same assembly after spacer removal.

Figure 46 is a top view of the grid structure (looking into the concave surface). Notice the virtually perfect concentricity and azimuthal alignment of the five sandwich layers. The slight eliptical appearance of the annular rings is due to a slight tilt of the assembly during photographing.

Figure 47 is a closer view with the assembly tilted somewhat to show the five layers. Tight "packing" of the sandwich is evident. It does appear, however, that on one side there is a small amount of separation between the screen grid and the screen to shadow grid spacer. This may be due to fluid pressure during machining as discussed earlier in section 4.2.3.

E2210
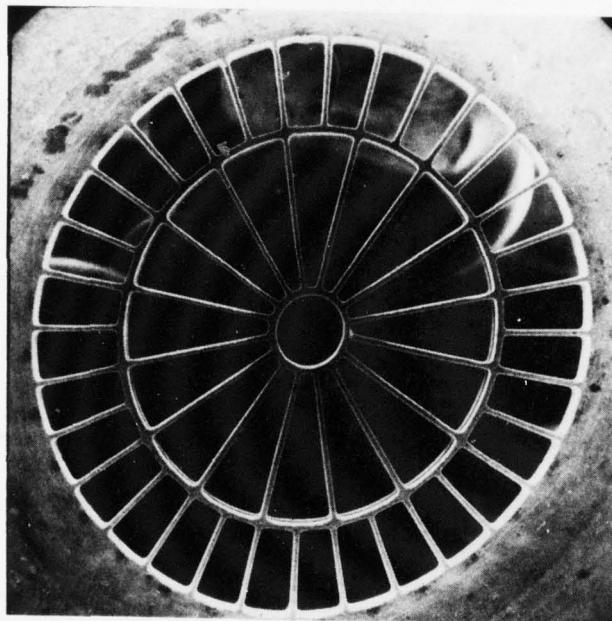
FIGURE 46   TOP VIEW OF SANDWICH GRID PRIOR
   TO SPACER REMOVAL

67

E2211
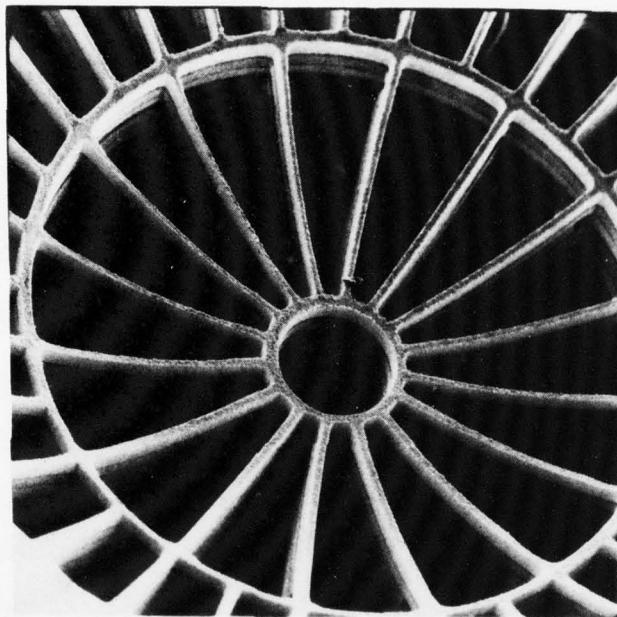
FIGURE 47 TILTED VIEW OF SANDWICH GRID
PRIOR TO SPACER REMOVAL

Figure 48 is a closeup of the small center ring. Its inside diameter is 0.023 inches.

Figure 49 is a photograph of the assembly after removal of the spacers. Notice the even spacing between the three large annular rings and the outer radial vanes. The material that looks like peeling skin is nickel plating that has not been cleaned off yet. The spacers in this assembly were removed with a 50% dilute solution of H_2SO_4 heated to $80^{\circ}C$.

Figure 50 is a side shot showing one of the flushing slots. Three grid surfaces separated by the spacer thickness are visible. Photomicrographs were not available at the writing of this report of the last assemblies processed with HCL. These appear quite brighter (cleaner) and show no peeling nickel.

The final results of this effort are three sandwich grid assemblies. Two have been partially processed with H_2SO_4 and show attack of the support ceramic. A demonstration of electrical isolation between the grids has not been achieved as of this writing. Final processing on this assembly was with HCL. The third assembly was processed completely with HCL and has demonstrated electrical isolation. This assembly also has some separation damage from fluid pressuring during the machining operation. In all assemblies, it appears that the control to screen grid spacing was reduced as a result of either pressure in pumping the acid through the assemblies or differential thermal contractions. This will be remedied in the future. A final problem which is now being worked on is the removal of residual chromium oxide left over from the spacers. Dry hydrogen firing will be attemped as a final cleanup operation.

E2212
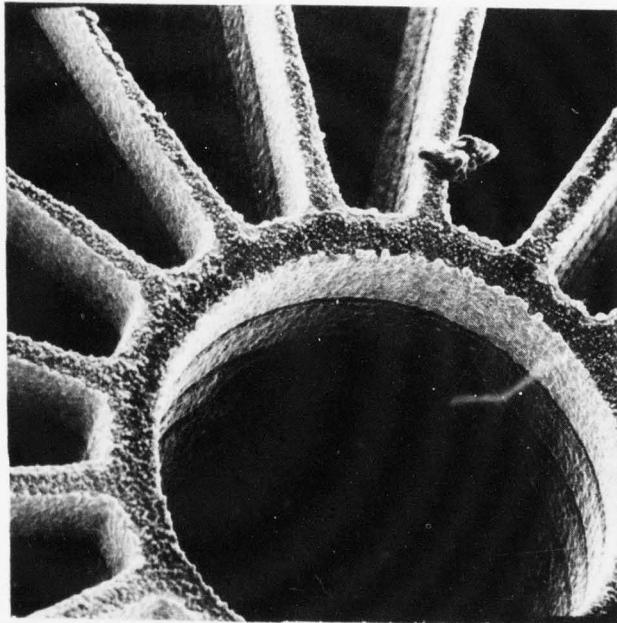
FIGURE 48   CLOSEUP OF CENTER ANNULAR RING
(i.d. = 0.023 INCHES) OF SANDWICH
GRID PRIOR TO SPACER REMOVAL

E2213
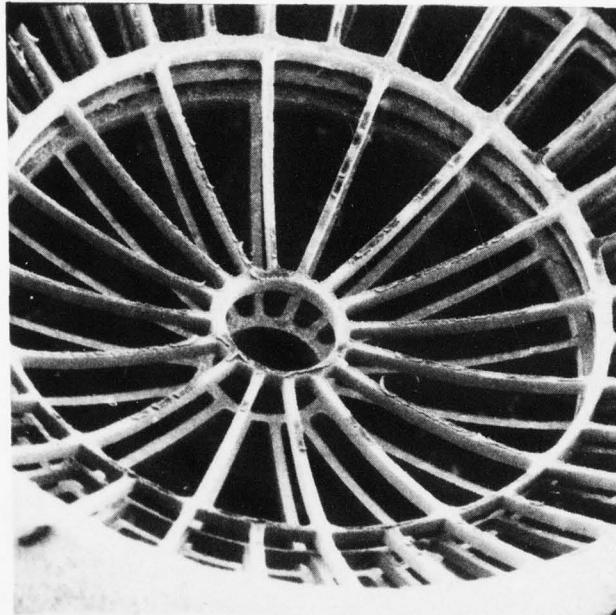
FIGURE 49   TILTED VIEW OF SANDWICH GRID
AFTER SPACER REMOVAL
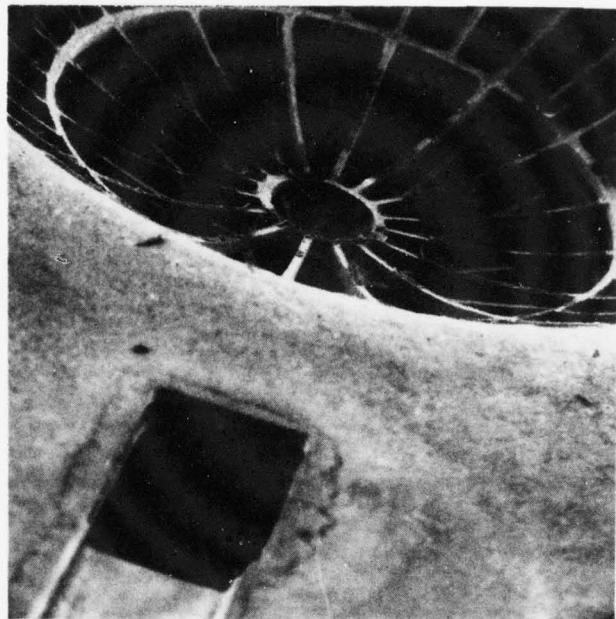
FIGURE 50   SIDE VIEW OF SANDWICH GRID AFTER
SPACER REMOVAL SHOWING ONE
OF THE FLUSHING SLOTS.

5.0 SUMMARY

The gun evaluation in section 3 clearly demonstrated a significant
variation in performance of the 4 guns. There was much evidence of
crooked grids and non-laminar beams. Furthermore, in the pulse mode
the respective beam shapes for each tetrode gun were radically differ-
ent. Tetrode #3 displayed a reduction of current in the beam tails
compared to that for tetrode #2. This difference was probably due to
the absence of screen grid vanes in tetrode #3. Finally, the beam
diameters in the CW mode from triode #5 compared most closely with those
from tetrode #3 since their grid structures were similar.

In an effort to reduce gun performance variations from gun to gun a new
grid assembly fabrication technique was developed. This "sandwich"
method development involved solving a number of design, tooling, and
processing problems to achieve the desired results. A few problems
remain which should be readily eliminated in the near future. These
include low machining yield, final cleaning of the assembly, and a
small change in grid spacing after final processing. The use of photo-
etched piece parts, hydrogen firing, and a modified spacer removal
operation or an alternate assembly configuration will be considered.

The grid assemblies which have been the result of this effort show
exceptional grid to grid concentricity, spacing consistency, and
azimuthal alignment – the goals of the effort. There is little doubt
that the results of using the "sandwich" assembly technique will result
in improved gun performance consistency.